Copy 5
RM E51L07

NACA RM E51L07

RESEARCH MEMORANDUM

ALTITUDE WIND TUNNEL INVESTIGATION OF HIGH-TEMPERATURE AFTERBURNERS

By E. William Conrad and Carl E. Campbell

Lewis Flight Propulsion Laboratory
Cleveland, Ohio

NATIONAL ADVISORY COMMITTEE
FOR AERONAUTICS

WASHINGTON

June 26, 1952

NATIONAL ADVISORY COMMITTEE FOR AERONAUTICS

RESEARCH MEMORANDUM

ALTITUDE WIND TUNNEL INVESTIGATION OF HIGH-TEMPERATURE AFTERBURNERS

By E. William Conrad and Carl E. Campbell

SUMMARY

An investigation was conducted in the NACA Lewis altitude wind tunnel to develop an afterburner producing the highest possible exhaust-gas temperatures and having suitable operational characteristics. In order to meet the requirements of military airplanes, maximum effort was concentrated on operation at near-stoichiometric fuel-air ratios. Most of the data were obtained at a nominal burner-inlet pressure of 2450 pounds per square foot; however, additional data were obtained at a nominal pressure level of 925 pounds per square foot.

By the use of adequate flame-holder blockage, long fuel-mixing lengths, and low burner-inlet velocities, and by careful matching of the fuel-injection pattern to the gas-flow pattern, performance approaching theoretical values was obtained with four series of burners having different diffuser inner-cone configurations. For example, at the design burner-inlet pressure level of 2450 pounds per square foot, the maximum exhaust-gas temperature obtained was 3900° R as compared with a theoretical maximum of slightly over 4000° R. Similarly, afterburner combustion efficiencies of at least 95 percent were obtained near maximum operating conditions. Combustion instability was encountered in several configurations; however, these difficulties were overcome by careful attention to flame-holder design and to aerodynamic designs of the diffuser.

Performance was obtained at a pressure level of 2450 pounds per square foot absolute using MIL-F-5572, MIL-F-5616, and MIL-F-5624 fuels. These fuels all gave almost identical performance results. The effects of two ceramic coatings on afterburner shell temperature were also studied. The results of one coating, Uverite, were inconclusive; however, a reduction in shell temperature of about 100° F was obtained with a coating formed by the use of 4-percent ethyl silicate in the afterburner fuel.

INTRODUCTION

During previous investigations of afterburning conducted at the NACA Lewis laboratory (references 1 to 4, for example), the objective

of obtaining high exhaust-gas temperatures and, consequently, maximum thrust augmentation was compromised to some extent in order to alleviate the problem of afterburner shell cooling. Because both cooling techniques used, (1) tail-pipe fuel stratification and (2) the use of a cooling liner, made some of the gases in the tail pipe unavailable for the burning of additional fuel, the maximum mean bulk exhaust-gas temperatures were about 3700° R. The transition in aircraft design from subsonic to supersonic flight regimes, in response to military needs, requires that the thrust potentialities of the afterburner be fully exploited. The primary objective of the investigation reported herein was therefore the attainment of maximum exhaust-gas temperature and thrust. In order to avoid the compromise on maximum exhaust-gas temperature imposed by the cooling techniques previously used, a secondary flow of cooling air was provided around the afterburner shell. Considerable effort was expended in solving problems of combustion instability. A brief study of shell cooling by means of ceramic coatings was also conducted.

The investigation was conducted with a full-scale axial-flow turbojet engine and an afterburner shell having dimensions consistent with the space requirements of supersonic research airplanes. Although the shell dimensions influenced some of the design compromises made, the methods used and the information obtained are nevertheless generally applicable. In all, over 40 configurations were studied. These configurations comprised numerous fuel-injection patterns in conjunction with four different diffusers and eight different flame holders. Data were obtained for most configurations at a nominal tail-pipe pressure of about 2450 pounds per square foot. Several of the more promising configurations were also operated at a burner-inlet pressure level of about 925 pounds per square foot. Because of the objective of obtaining high exhaust-gas temperatures, most of the data were obtained at afterburner fuel-air ratios from about 0.05 to 0.09. A few configurations, however, were also operated at much lower fuel-air ratios.

In order to obtain high efficiency at high fuel-air ratios, very precise tailoring of the fuel pattern was required to obtain a uniform mixture over the entire cross section of the afterburner. The problem of obtaining maximum temperature was also facilitated by the relatively low burner-inlet velocity of about 400 feet per second. Such low velocities, however, tend to aggravate combustion stability difficulties. Three approaches to the stability problem were investigated: (1) the use of good aerodynamic design in the diffuser section to eliminate regions of flow separation, (2) the use of high velocities in the diffuser section to prevent flame propagation upstream of the flame holder, and (3) the use of flame holders designed to reduce the volume of combustible regions which detonate under certain conditions of fuel-air ratio, pressure, and temperature.

APPARATUS AND INSTRUMENTATION

Engine

The J34-WE-30 engine used in this investigation has a sea-level static-thrust rating of 3150 pounds at a turbine-outlet temperature of about 1200° F and a rated engine speed of 12,500 rpm. At this condition, the air flow is about 58 pounds per second. The engine has an 11-stage axial-flow compressor with a pressure ratio of about 4.0 at rated conditions, a double-annulus combustor, and a two-stage turbine.

Installation

The engine was mounted on a wing section that spanned the 20-foot-diameter test section of the altitude wind tunnel (fig. 1). Engine inlet-air pressures corresponding to altitude flight conditions were obtained by introducing dry refrigerated air from the tunnel make-up air system through a duct to the engine inlet. A slip joint with a frictionless seal was used in the duct, thereby making possible the measurement of thrust and installation drag with the tunnel scales. Air was throttled from approximately sea-level pressure at the engine inlet, while the static pressure in the tunnel test section was maintained to correspond to the desired altitude. In order to simplify the installation, no cowling was installed. Cooling air was supplied to a shroud around the afterburner by means of a duct through the trunion and the wing. The cooling air was throttled from atmospheric conditions to regulate the cooling mass flow. No attempt was made to correlate either the pressure or temperature of the cooling air with the engine operating condition or flight condition.

Instrumentation

Instrumentation for measuring pressures and temperatures was installed at several stations throughout the engine and afterburner as indicated in figure 2. Air flow was determined from measurements of pressure and temperature at station 1 in the make-up air duct. A comprehensive pressure and temperature survey was obtained at the turbine outlet, station 5. Diffuser pressure losses for the series-C configurations were determined by a single rake of 8 total-pressure tubes at station 6. Total and static pressures 2 inches upstream of the exhaust-nozzle outlet were measured by means of a water-cooled survey rake which was mounted so that the rake drag could be measured by a pneumatic capsule.

Afterburner shell temperatures were obtained with from 10 to 16 thermocouples welded into the skin a few inches upstream of the exhaust-nozzle inlet. Cooling-air temperatures were obtained from 3 thermocouples

in each plenum chamber. The symbols and the methods of calculation used in this report are given in the appendix.

AFTERBURNERS

Afterburner Shell

Detailed dimensions of the afterburner shell and the cooling shroud used throughout the investigation are given on the cross-sectional sketch of figure 3. The assembly consisted of four sections: (1) a diffuser section 24 inches long, tapering from an inlet diameter of 21 inches to an outlet diameter of $25\frac{1}{2}$ inches; (2) a cylindrical section 23 inches long used for diffusion or to provide fuel-mixing length; (3) a combustion chamber with an over-all length of 61 inches which comprised a cylindrical section 33 inches in length followed by a 28-inch-long section with an outlet diameter of 21 inches; and (4) a water-cooled conical nozzle section 4.67 inches in length with an outlet diameter of $20\frac{3}{32}$ inches.

Most of the combustion-chamber length was surrounded by a shroud which provided a uniform 1/2-inch passage height for the cooling air. Plenum chambers were provided at both ends of the shroud to permit the use of either parallel-flow or counter-flow cooling. Except for a few runs, counter-flow cooling was used throughout the program. The cooling air entered and was discharged from the installation in a radial direction to eliminate any contribution to the thrust measured by the tunnel scale system.

Design Considerations

As mentioned previously, both the approximate diameter and length of the burner shell were determined by the space requirements of typical supersonic research airplanes. The average value of burner-inlet velocity was, of course, fixed by this specification of the burner diameter. The axial position of the flame holder was chosen on the basis of previous experience (reference 4, for example) to permit the longest burning length feasible without imposing undue cooling problems in the flight installation. The many configurations are grouped into four series, as shown in figure 4, on the basis of the type of diffuser inner cone. For the first three series, the flame holder was located 64 inches upstream of the exhaust-nozzle outlet as shown by the broken line. For the fourth series, the flame holder was located a few inches farther upstream.

In series A configurations (fig. 4), the diffuser inner cone supplied by the engine manufacturer was used in order to minimize delay in production in the event that satisfactory performance results could be

obtained. Because of the relatively blunt shape of the production inner cone, flow separation from the surface was anticipated. Such separation is undesirable from considerations of combustion stability, as discussed in a later section, and also from a performance viewpoint. In an effort to reduce or to eliminate anticipated flow separation, a row of vortex generators (reference 5) was therefore used on the production diffuser inner cone in the B-series configurations. As a further effort to improve velocity distribution and pressure recovery in the diffuser, another inner cone was constructed to reduce the rate of diffusion. This inner cone, used with series-C configurations, was also provided with vortex generators throughout most of the investigation. The vortex generators used with series B and C comprised 18 symmetrical noncambered airfoils of 1/2-inch span and 2-inch chord. As shown by the sketch of figure 5, the airfoils were staggered alternately at an angle of 13° to the flow direction. Series-D configurations, which were considered an alternate solution to the instability problem, were designed on the theory that no flash back would occur if boundary velocities were maintained at a level sufficiently high to prevent burning near the diffuser inner cone; this was accomplished by using very little diffusion upstream of the flame seat to keep the mean velicity high and to avoid separation. A step-type flame-seat area was constructed on the diffuser inner cone to provide a stable flame at the location farthest upstream where burning was likely to occur.

In all configurations, the fuel was injected as far upstream of the flame holder as appeared feasible to permit the maximum time for fuel mixing and evaporation. For series A, B, and C the fuel was injected at or very near the downstream end of the diffuser inner cone to prevent the occurrence of combustible mixtures in possible regions of separation on the inner cone. For series D, the farthest upstream location possible for fuel injection was limited by the location of the instrumentation at the turbine outlet. The plane of fuel injection used with each series is indicated in figure 4.

The fuel system was so designed that configurations, comprising different patterns of fuel injection orifices, could be selected remotely. Selection was made possible by use of two sets of 12 radial spray bars, each with a different fuel-spray pattern, that could be used independently or simultaneously. Thus, three fuel-spray patterns were obtainable for any one installation. The spray bars were constructed of 5/16-inch Inconel tubing flattened to a thickness of about 1/8 inch. Holes varying in size from 0.016 to 0.040 inch were drilled in the flat sides of the spray bars thus ejecting fuel normal to direction of gas flow. The fuel-distribution patterns which gave optimum performance for each of the four series of configurations are given in figure 6. The shaded areas shown represent areas occupied by the diffuser inner cone.

Five flame holders were used in conjunction with series A, B, and C. Details of these flame holders are given in figure 7. Flame holders 1 and 2 were of more or less conventional design; however, corrugations were used on the gutter of flame holder 1 to increase the flame seat perimeter. The gutters of flame holder 2 were constructed with the outer side parallel to the combustion-chamber wall in accordance with observations made elsewhere that such a gutter shape has a beneficial effect on shell temperatures. Flame holders 3, 4, and 5 were designed to improve combustion stability. The stability considerations involved will be discussed in a later section.

The three flame-seat configurations shown in figure 8 were used with series D. In order to eliminate overheating of the juncture between the step on the inner cone and the center pilot, the inner cone of flame holder 6 was shortened to form flame holder 7. In an effort to improve performance at lower pressure levels, additional blockage, in the form of radial struts, was added to form flame holder 8.

A device called a temperature ladder was used to determine the uniformity of the exhaust-gas temperature. This device (fig. 9) comprised a 1/2-inch water-cooled Inconel tube spanning the diameter of the combustion chamber about 1 foot upstream of the exhaust-nozzle outlet. Pieces of 1/8-inch-diameter welding rod of uniform length were butt-welded to the tube at spacings of about 1 inch. When in use, the tube was so mounted that one end bar was about 1/4 inch from the wall and the other end bar was a few inches across the burner center line. Local temperature profiles were apparent by visual comparison of the color variations of the rods during afterburner operation. These observed temperature variations were used to guide modifications to the fuel-injection pattern.

Engine and afterburner fuel flows were measured by calibrated rotameters. The fuel used in the engine was clear gas, MIL-F-5572 (AN-F-48b). The afterburner fuel used during most of the running was MIL-F-5616 (AN-F-32), which had a lower heating value of 18,670 Btu per pound. A few comparative runs were made using clear gas, MIL-F-5572 (AN-F-48b) and MIL-F-5624 (AN-F-58) in the afterburner.

Procedure

As noted in the INTRODUCTION, data were obtained at nominal pressure levels in the afterburner of 2450 and 925 pounds per square foot absolute. The high pressure was simulated by operation at rated engine speed, an altitude of 25,000 feet, and an inlet ram-pressure ratio of 1.7. Data at the lower pressure were obtained by operation at rated engine speed, an altitude of 45,000 feet, and a ram-pressure ratio of 1.6. Inasmuch as a fixed-area exhaust nozzle was used, the burner-inlet pressure and

temperature varied with the amount of burning so that the values given herein are averages. For any given afterburner fuel-air ratio, the turbine-outlet conditions with the four diffuser configurations discussed in detail were about equal inasmuch as combustion efficiencies were almost equal. Most of the data were obtained near the maximum afterburning condition inasmuch as the objective of the study was the attainment of high exhaust-gas temperatures.

With each diffuser inner cone and flame-holder configuration, a series of configurations comprised of changes in radial fuel distribution were studied. The first distribution was based on either the velocity profile of the gas obtained in the diffuser during an earlier investigation, or on the results obtained on the previous configurations in the investigation reported herein. Almost invariably the first estimated distribution was not optimum because changes in the shape of either the inner cone or the flame holder influenced the mass-flow distribution at the diffuser outlet. Observations of the temperature ladder showed the radial locations at which the exhaust gas was relatively cool. By observation of the change in temperature of these strata as the over-all fuel-air ratio was changed, it was determined whether these strata were excessively rich or lean, and the fuel-injection pattern was altered accordingly. The use of this technique made possible the attainment of a practical, optimum radial distribution in four or five attempts. Daily checks were made on the relative performance of each configuration to confirm the performance trends indicated by the temperature ladder and also to indicate the point of diminishing return in any line of development.

RESULTS AND DISCUSSION

As mentioned in the INTRODUCTION, a large number of configurations were obtained by variations in the diffuser inner cone, the flame holder, or the fuel-injection pattern. Because the objective of the investigation was the attainment of maximum exhaust-gas temperature, performance results are shown only for the best combination of fuel pattern and flame holder for each of the four series of configurations. Therefore, unless otherwise noted, configurations denoted by the letters A to D will denote the optimum combination of fuel pattern and flame holder in the series indicated. It should be noted that for operation with the uniform fuel-air-ratio distribution used during this study, the variations in flame-holder design had little effect on performance; the effects on combustion stability were, however, important and, as will be discussed, resulted in unsatisfactory operational characteristics for two of the four series.

Performance

Combustion. - The combustion performance of the various configurations is considered in terms of the mean bulk exhaust-gas temperature and the combustion efficiency. Tail-pipe combustion efficiency is defined as the ratio of the actual enthalpy rise to the enthalpy rise theoretically possible. The numerator may be obtained within experimental accuracy by use of the equations given in the appendix and the measured values of scale thrust, turbine-outlet temperature, and total pressure at the exhaust-nozzle outlet. For the fuel used, the maximum exhaust-gas temperature theoretically available without dissociation is about 4250° R, and the maximum value including dissociation based on the data of reference 6 is slightly over 4000° R. Because of the state change of the gases in expanding through the exhaust nozzle, the chemical equilibrium is changed and some of the energy made unavailable by dissociation is recovered and produces thrust. Hence, the true theoretical temperature lies somewhere between the two values. Determination of the exact value, however, is laborious and is unwarranted for the purposes of this paper. Combustion efficiencies presented herein are therefore based on a theoretical temperature that includes dissociation. This value, obtained by the use of reference 6, may therefore be slightly high. This error in the direction of high combustion efficiency is, however, balanced somewhat by the omission of a heat loss to the cooling air which would raise the combustion efficiency 1 or 2 percent.

Results obtained for series A are given in figure 10 where mean bulk exhaust-gas temperature and afterburner combustion efficiency are shown as functions of afterburner fuel-air ratio. At a nominal burner-inlet pressure level of 2450 pounds per square foot absolute, the maximum exhaust-gas temperature obtained was about 3880° R. At this operating condition the afterburner fuel-air ratio was about 0.07 and the afterburner combustion efficiency was about 0.97, which was very near the peak efficiency obtained. At the lower pressure level of 925 pounds per square foot absolute, the maximum values of exhaust-gas temperature and afterburner combustion efficiency were reduced to 3500° R and 0.87, respectively.

The results for the best configuration of series B are presented in figure 11. At a pressure level of 2450 pounds per square foot absolute, both the maximum exhaust-gas temperature and the peak afterburner combustion efficiency were the same as for series A. The performance of series B deteriorated somewhat more with increased altitude than series A with the result that the peak exhaust-gas temperature was reduced to 3380° R at the lower pressure level of 925 pounds per square foot absolute, and the peak combustion efficiency was reduced to about 0.84.

Results obtained with series C are presented in figure 12 for operation at a pressure level of 2450 pounds per square foot. Within the

range of experimental accuracy, the peak values of exhaust-gas temperature and afterburner combustion efficiency were again about the same as the values obtained for series A and B.

Data are presented in figure 13 to show the combustion performance obtained with series D. At the higher pressure level, the maximum exhaust-gas temperature obtained was 3900° R. Maximum afterburner combustion efficiency was about 0.98. At the lower pressure level, the maximum exhaust-gas temperature was 3620° R and the peak afterburner combustion efficiency was about 0.91.

The combustion performance of the four series is compared in figure 14 for operation at a pressure level of 2450 pounds per square foot absolute. Despite the widely divergent flame-holder, diffuser, and fuel-pattern designs used, the optimum performance obtained was different by only a few percent. This result is not surprising inasmuch as adequate flame-holder blockage, long fuel-mixing lengths, and low burner-inlet velocities were incorporated in all the series and the fuel-injection pattern was optimized. It may therefore be concluded that for operation at a pressure level of about 1 atmosphere, combustion performance is primarily dependent on optimum matching of the fuel-injection pattern and the air-flow-distribution pattern. The maximum theoretical temperature curve has been superimposed on figure 14 to indicate the magnitude of possible future improvements. At a pressure level of 925 pounds per square foot absolute, however, optimization of the fuel pattern was not the entire answer. As illustrated by figure 15, changes in diffuser and flame-holder geometry produced an appreciable difference in performance despite optimization of the fuel-injection pattern. This is in accord with the data of reference 4, where it is shown that variations in flame-holder blocked area or combustion-chamber length became of increasing importance as the altitude was increased (or pressure level reduced).

Pressure-loss characteristics. - It will be realized, of course, that the parameters of exhaust-gas temperature and afterburner combustion efficiency which were chosen to present the combustion performance are not directly translatable into thrust and specific fuel consumption without consideration of the pressure losses in the afterburner. The pressure-loss characteristics for the four basic series of afterburners are given in figure 16(a) where the total-pressure drop from the turbine outlet to the exhaust-nozzle outlet, expressed as percentage of the impact pressure at the turbine outlet, is shown as a function of the afterburner fuel-air ratio. Over the entire fuel-air-ratio range, the maximum pressure-loss factor $\Delta P/q$, obtained with series D, was about 0.2 greater than the minimum value obtained with series C. The effect of these pressure-loss characteristics on thrust cannot be shown by a direct comparison of thrust curves because the data of series C in particular were affected by a slight deterioration in basic engine performance. The physical significance of these pressure losses is given,

however, in figure 16(b) where augmented net-thrust ratio is presented as a function of the afterburner pressure-loss coefficient for operation at an altitude of 25,000 feet and a flight Mach number of 0.92. From the data of figures 14 and 16 it may be concluded that the thrust obtained from each of the four series was about the same at the high-pressure level, inasmuch as the differences in pressure drop were not large and the higher pressure drop for series D was balanced by a higher exhaust-gas temperature.

The constancy of the pressure-drop-coefficient data of figure 16(a) is difficult to explain in view of the increase in momentum pressure loss which accompanies any increase in the amount of heat added to the gases in the combustion process. In view of the large amount of data (most of which are not presented) which show this trend, it can only be concluded that the friction pressure drop decreases as the afterburner fuel-air ratio increases. A possible explanation for such behavior might be the reduction of flow separation in the diffuser accompanying an increase in flow resistance at the diffuser outlet.

Over-all performance. - In order to indicate further performance gains that may be possible, the net thrust and net-thrust specific fuel consumption are shown in figure 17 for a series-D configuration operating at an altitude of 25,000 feet at a flight Mach number of 0.92. Superimposed are theoretical curves which show the performance possible if friction pressure losses were reduced to zero and afterburner combustion efficiency was 1.00. The data show the actual maximum thrust to be 91 percent of the theoretical maximum; however, not all of the 9 percent difference may be recovered inasmuch as the friction pressure drop cannot be reduced to zero. The extent to which the specific-fuel-consumption margin may be reduced by improvements in combustion efficiency is indicated by the earlier figures. It should be noted that momentum pressure losses were retained in the theoretical calculations inasmuch as such losses cannot be greatly reduced with burners of practical dimensions.

Effect of vortex generators. - As shown by the data of figure 16(a), the installation of vortex generators (configuration B) on the production diffuser inner cone (configuration A) somewhat increased the over-all pressure loss. On the other hand, the installation of vortex generators on the inner cone of series C reduced the pressure losses in the diffuser about 45 percent. It therefore appears that vortex generators are helpful in reducing pressure losses in marginal areas but also that they are not a substitute for good aerodynamic diffuser design.

The installation of vortex generators on both the production inner cone and the inner cone of series C caused a change in the air-flow distribution of sufficient magnitude that changes in the fuel-injection pattern were required to again obtain optimum performance. The effect on diffuser-outlet velocity of vortex generators with the series C inner cone is shown in figure 18. The maximum velocity was reduced about

[redacted]

100 feet per second and also the velocity near the diffuser inner cone was increased from 0 to about 300 feet per second. Not only are the conditions for combustion improved by the reduction in peak velocity, but also the tendency for flash back near the inner cone is reduced by elimination of the very low-velocity region.

Effect of fuels. - A small amount of data was obtained with two of the series C configurations at a pressure level of 2450 pounds per square foot absolute to determine the performance obtainable with three different fuels. Data are shown for one configuration in figure 19(a), where performance of MIL-F-5572 and MIL-F-5616 fuels is compared. Similar data are shown for another configuration in figure 19(b) for operation with MIL-F-5616 and MIL-F-5624 fuels. From these data, it appears that for fuel-mixing lengths of about 24 inches, burner performance is practically identical for the three fuels tested. As noted in reference 7, however, the effects of fuel volatility are appreciable when fuel-mixing lengths on the order of 8 inches are used.

Operational Characteristics

Combustion instability. - Over a period of several years, numerous investigations of afterburners have been conducted at the NACA Lewis laboratory and several hundred configurations have been studied. In these investigations, combustion instability occurred numerous times. Experience indicates that combustion instability may be classified in three groups, on the basis of frequency. These groups are identified by the names, rumble, buzz, or screech, depending on the frequency and magnitude of the associated pressure pulses. The circumstances under which these forms of instability are encountered and the measures used to prevent their occurrence will be discussed in the following paragraphs.

The type of combustion instability referred to as rumble is usually caused by explosions of large pockets of combustible mixture. This violent instability usually occurs at frequencies of less than one to a few cycles per second, and generally occurs only for a few cycles at ignition of the burner or near either rich or lean blow-out. During starts, observations through windows in the burner shell indicated that the rumble is due to flash back into the fuel-mixing zone upstream of the flame holder; near the blow-out limits it is probably caused by the blow-out and reignition of local pockets of fuel-air mixture, at or downstream of the flame holder, that momentarily exceed the combustible limits of fuel-air ratio. This type of burning appears to be associated with configurations having uniform fuel-air patterns and could probably be avoided or reduced in severity at ignition by suitable stratification of the fuel. Rumble was encountered for a few cycles upon ignition and preceeding either rich or lean blow-out for practically all the configurations used in the investigation reported herein. Although no

quantitative measurements were obtained in the present study, it is noted in reference 8 that pressure pulsations as high as ±9 pounds per square inch have been encountered in afterburner operation, presumably during rumble.

Buzzing is a term used to denote combustion which produces pressure pulsations of intermediate frequency on the order of perhaps 10 to 50 cycles per second. High-speed schlieren motion pictures of a two-dimensional ram-jet model with transparent walls have provided an understanding of this type of instability as follows:

(a) Upon ignition, a flame front fans out from each flame stabilizer and intersects either a wall or the flame front from the adjacent flame stabilizer at a point some distance downstream.

(b) A curved flame front starts at the point of intersection and travels upstream with increasing velocity through the wedge-shaped pocket of combustibles bounded by the intersecting flame fronts.

(c) The curved flame front progresses to a point somewhat upstream of the flame holder, whereupon combustion ceases. The pressure pulse produced by this curved flame front momentarily stops or reverses the direction of flow of the gas column.

(d) Following dissipation of the pressure pulse, the flow is re-established and a fresh charge of combustible mixture displaces the burner charge, whereupon ignition occurs and the cycle repeats.

Pressure pulsations of this type were encountered for all configurations in series A and B except at fuel-air ratios above about 0.065. These pulsations were usually of such severity that extreme damage to the afterburner structure occurred when buzzing was allowed to persist more than a few minutes. Consequently, both series A and B configurations must be regarded as unsatisfactory from an operational viewpoint. It should be noted that only the three flame holders shown in figures 7(a), 7(b), and 7(c) were used in series A and B. Buzzing combustion was also encountered with these flame holders in series C; however, the three-element flame holders shown in figures 7(d) and 7(e) produced smooth combustion in series-C configurations except very near the lean blow-out condition. These flame holders were designed to avoid buzzing by reducing the volume of the wedge-shaped regions between adjacent flame sheets and may have operated smoothly in series A and B had they been tried.

Screeching or screaming combustion is generally encountered at high burner-inlet pressures when low-velocity regions such as separation regions or wakes exist in the fuel-mixing zone. Measurements from two sources show that screeching combustion occurs at frequencies from 1200 to 6000 cycles per second. This type of combustion was observed in the

[redacted]

study reported herein, to exist on the surfaces of diffuser inner cones and evidence has been obtained in other investigations to show that it may occur on the lee side of support struts or on the outer wall of the diffuser. In the configurations which led to the development of the series-D configurations, screeching was observed at all altitudes up to and including 35,000 feet, and severe damage occurred when it was allowed to continue for more than a few minutes. This type of instability was believed to be due to the rapid burning or detonation of small pockets of combustible mixtures along the upstream edge of a low-velocity region in which more or less stable combustion was occurring. It was reasoned that the detonation of these fringe pockets produced pressure pulse which delayed the introduction of a fresh charge. Following the consumption of the fuel and the dissipation of the pressure pulse, a new charge flowed into the detonation-susceptible region, whereupon detonation again occurred. This concept of detonation is substantiated by the high values of flame speed reported in reference 9, where flame velocity was found to increase from 500 feet per second at a distance 5 inches upstream of the ignition source to 3000 feet per second 24 inches upstream. Such flame velocities can probably be explained only on the basis of detonation. These values also imply a rather low velocity near the flame holder where upstream propagation of the flame begins.

In the development of the series-D burners, two methods were used to eliminate the screeching. These methods and the reasons for their use were as follows: (1) Screeching was definitely due to the existence of a region of burning (which to the eye appeared stable) on the surface of the diffuser inner cone immediately upstream of the pilot cone which probably served as an ignition source. Conditions for combustion were such that combustion was easily supported at the downstream end of the inner cone, but the location of the upstream edge is believed to be determined by the local gas velocity. Increasing the local approach velocity by proper aerodynamic design either to avoid flow separation or to increase the mean gas velocity would, if increased enough, prevent the initial upstream flame propagation and hence eliminate the burning along this surface. This method was applied and the marked success achieved served to support the theory advanced. (2) Inasmuch as the pressure pulsations were attributed to irregularities in the combustion at the upstream fringe of the area, it seemed likely that the provision of a stable flame seat in the fringe area would eliminate the pulsations. In order to accomplish this stability, a step-type flame seat was used on the diffuser inner cone. Again the screeching was eliminated. In series-D configurations, both high approach velocities (method (1)) and stable flame seats (method (2)) were used.

Shell cooling. - As shown in figure 3, cooling air was passed around the burner shell through a 1/2-inch annular space between the shell and the shroud. During most of the investigation counter-flow cooling was used as a conservative test measure. A few runs were made, however,

with parallel flow of the cooling air. Average shell temperatures at the exhaust-nozzle inlet are shown in figure 20 as a function of cooling-air mass-flow ratio for both methods. At reasonable values of the cooling-flow ratio, on the order of 0.10, temperatures were excessive particularly for the more practical parallel flow. As a result, ceramic coatings were used in an effort to reduce shell temperatures.

Two types of ceramic coatings were applied to the inside of the burner shell to reduce shell temperatures. The primary purpose of both was to reduce the heat flux due to radiation by reducing the absorptivity of the shell. In reference 10, it is shown that a coating of Uverite reduced the absorptivity of a wall to about 0.10 of that for stainless steel at a wall temperature of 1000° F and about 0.13 at a wall temperature of 1600° F. Uverite powder, which is composed of the oxides of calcium, antimony, and titanium was mixed with sodium silicate and painted on the inside of a burner shell which had been blast-cleaned with metal-grit particles to remove any grease or other foreign material. Inasmuch as time did not permit the recommended bake period, the engine was operated without afterburning for about 1 hour to cure the coating before the burner was used. Perhaps as a consequence of the improper bake treatment, the coating flaked off in large areas (fig. 21) after only a few minutes of operation. In the relatively hot portion of the burner, where the shell thermocouples were installed, the coating was almost completely gone and no measurable difference in shell temperature was obtained.

Another approach to the problem was the use of a 4-percent solution of ethyl silicate in the afterburner fuel. The coating of silicon was expected to flake off continually and be replenished by plating-out of more silicon from the fuel. As shown in figure 22, a heavy coating formed within the flame-holder gutters and a thin frosty coating formed on the hotter portions of the burner shell. In operation, the inside of the shell had a somewhat milky appearance as contrasted to the clear orange-red color of the uncoated shell. Because of rough burning just prior to running the ethyl silicate, only four of the original 16 thermocouples on the shell were operative when the ethyl silicate was used. The individual readings of these four thermocouples are shown in figure 23 for operation at identical conditions before the ethyl silicate was used, while it was used, and after its use. It appears from these data that the shell temperature was reduced about 100° F and also that the coating was effective for at least the remaining 15 minutes of burning after running was resumed on clear fuel. Additional data are required, however, to establish the length of time during which this type of coating may be effective after operation with untreated fuel is resumed.

CONCLUDING REMARKS

By provision of adequate flame-holder blockage, long fuel mixing lengths, and low burner-inlet velocities, and by careful matching of the fuel-injection pattern to the gas-flow pattern, performance approaching theoretical values was obtained with four series of burners having different diffuser inner-cone configurations. For example, the maximum exhaust-gas temperature obtained was about 3900° R as compared with a theoretical maximum of slightly over 4000° R. Similarly, at the design pressure level of 2450 pounds per square foot absolute, afterburner combustion efficiency was at least 95 percent in the range of afterburner fuel-air ratios which produced maximum exhaust-gas temperature.

The requirements of long fuel-mixing length and low burner-inlet velocity conflict with the requirements for combustion stability. Suitable combustion stability was nevertheless achieved with two configurations over the entire operable range of flight conditions by careful attention to the aerodynamic design of the diffuser and careful consideration of the combustion characteristics of various flame-holder designs.

Performance data with three fuels, MIL-F-5572, MIL-F-5616, and MIL-F-5624, were obtained at a nominal pressure level of 2450 pounds per square foot. No effect on performance was apparent. The effects of two ceramic coatings, Uverite and silicon, on shell cooling were also studied briefly. Because of inadequate time for preparation, the Uverite coating results were inconclusive; however, the addition of 4-percent ethyl silicate to the afterburner fuel produced a coating which reduced shell temperatures about 100° F.

Lewis Flight Propulsion Laboratory
National Advisory Committee for Aeronautics
Cleveland, Ohio

APPENDIX - CALCULATIONS

SYMBOLS

The following symbols are used in this report:

A	cross sectional area, sq ft
B	thrust-scale reading, lb
C_V	velocity coefficient, ratio of scale jet thrust to rake jet thrust
D	external drag of installation, lb
D_r	drag of exhaust-nozzle survey rake, lb
F_j	jet thrust, lb
F_n	net thrust, lb
f/a	fuel-air ratio
g	acceleration due to gravity, 32.2 ft/sec^2
H_a	total enthalpy of air or gas mixture, Btu/lb
P	total pressure, lb/sq ft absolute
p	static pressure, lb/sq ft absolute
$\Delta P/q$	ratio of total-pressure loss across afterburner due to friction and heat addition to inlet impact pressure, $(P_5-P_7)/P_5-p_5)$
R	gas constant, ft-lb/(lb)(^oR)
T	total temperature, ^oR
t	static temperature, ^oR
V	velocity, ft/sec
W_a	air flow, lb/sec
W_f	fuel flow, lb/hr
W_g	gas flow, lb/sec

[redacted]

$\frac{W_{f,t}}{F_{n,s}}$	specific fuel consumption based on total fuel flow and scale net thrust, lb/(hr)(lb thrust)
γ	ratio of specific heats for gases
η	combustion efficiency
λ	total enthalpy of fuel, Btu/lb

Subscripts:

a	air
ab	afterburner
e	engine
f	fuel
i	indicated
j	jet
n	exhaust-nozzle exit
s	scale
x	inlet duct at frictionless slip joint
0	free-stream conditions
1	engine-inlet duct
5	afterburner inlet (turbine outlet)
7	exhaust nozzle, 2 inches upstream of water-cooled nozzle-extension outlet

Methods of Calculation

Temperatures. - Static temperatures were determined from thermocouple indicated temperatures with the following relation:

$$t = \frac{T_1}{1 + 0.85\left[\left(\frac{P}{p}\right)^{\frac{\gamma-1}{\gamma}} - 1\right]} \tag{1}$$

where 0.85 is the impact recovery factor for the type of thermocouple used. Total temperatures were determined by the adiabatic relation between temperatures and pressures.

Airspeed. - The equivalent airspeed was calculated from ram-pressure ratio by the following equation with complete pressure recovery at the engine inlet assumed:

$$V_0 = \sqrt{\frac{2\gamma_1 gRT_1}{\gamma_1 - 1}\left[1 - \left(\frac{p_0}{P_1}\right)^{\frac{\gamma_1-1}{\gamma_1}}\right]} \tag{2}$$

Air flow. - Air flow was determined from pressure and temperature measurements in the engine inlet-air duct by the following equation:

$$W_{a,1} = p_1 A_1 \sqrt{\frac{2\gamma_1 g}{Rt_1(\gamma_1 - 1)}\left[\left(\frac{P_1}{p_1}\right)^{\frac{\gamma_1-1}{\gamma_1}} - 1\right]} \tag{3}$$

Gas flow. - The total weight flow of fuel and air through the engine and afterburner was calculated as follows:

$$W_{g,8} = W_{a,1} + \frac{(W_{f,e} + W_{f,ab})}{3600} \tag{4}$$

Afterburner fuel-air ratio. - The afterburner fuel-air ratio is defined as the ratio of the weight flow of fuel injected in the afterburner to the weight flow of unburned air entering the afterburner from the engine. Weight flow of unburned air was determined by assuming that the fuel injected in the engine was completely burned. This assumption of 100-percent combustion efficiency in the engine results in only a small error in afterburner fuel-air ratio because the engine was operated where η_e is known to be high. Afterburner fuel-air ratio was calculated from the equation:

$$(f/a)_{ab} = \frac{W_{f,ab}}{3600\, W_{a,1} - \frac{W_{f,e}}{0.067}} \tag{5}$$

where 0.067 is the stoichiometric fuel-air ratio for the engine fuel.

[redacted]

Exhaust-gas total temperature. - The total temperature of the exhaust gas was calculated from the exhaust-nozzle outlet total pressure, scale jet thrust, velocity coefficient, and gas flow by means of the following equation:

$$T_j = \left(\frac{F_{j,s}}{C_V}\right)^2 \left(\frac{g}{2R}\right) \left(\frac{\gamma_7 - 1}{\gamma_7}\right) \left\{ \frac{1}{W_{g,7}^2 \left[1 - \left(\frac{p_0}{p_7}\right)^{\frac{\gamma_7 - 1}{\gamma_7}}\right]} \right\} \qquad (6)$$

Values of the gas constant R were determined from the fuel-air ratio and the hydrogen-carbon ratio of the fuel according to the method of reference 11. The velocity coefficient C_V, which is defined as the ratio of scale jet thrust to rake jet thrust, was determined to be 0.97 from data presented in reference 12.

Combustion efficiency. - Afterburner combustion efficiency as presented in this report is defined as the actual enthalpy rise through the afterburner to the enthalpy rise that could be obtained with the theoretical maximum exhaust-gas temperature determined by the method of reference 6. This reference provides charts for determining the temperature obtainable with ideal combustion including the effects of dissociation. This temperature is based on fuel-air ratio, burner inlet temperature, hydrogen-carbon ratio of the fuel, lower heating value of the fuel, and the products of combustion from the initial burning process in the engine combustors.

The actual increase in enthalpy through the afterburner is expressed as

$$(W_{g,7}H_7 - W_{g,5}H_5) = (3600\, W_{a,1}H_{a,7} + W_{f,ab}\lambda_{ab,7} + W_{f,e}\lambda_{e,7}) - (3600\, W_{a,1}H_{a,5} + W_{f,e}\lambda_{e,5})$$

where the enthalpy values at station 7 are based on the actual exhaust gas temperatures from equation (6). The maximum enthalpy rise obtainable is determined from the preceding relation with enthalpy values at station 7 based on the theoretical maximum exhaust-gas temperature. The resulting expression for combustion efficiency is therefore:

$$\eta_{ab} = \frac{3600\, W_{a,1}(H_{a,T_j} - H_{a,5}) + W_{f,e}(\lambda_{e,T_j} - \lambda_{e,5}) + W_{f,ab}\lambda_{ab,T_j}}{3600\, W_{a,1}(H_{a,T_{max}} - H_{a,5}) + W_{f,e}(\lambda_{e,T_{max}} - \lambda_{e,5}) + W_{f,ab}\lambda_{ab,T_{max}}} \qquad (7)$$

[redacted]

The enthalpies of the products of combustion were determined from temperature-enthalpy charts for air and from temperature-enthalpy charts for fuels having the same hydrogen-carbon ratios as the fuels used in this investigation (see reference 13). The charts used for obtaining fuel enthalpies were based on a fuel-inlet temperature of 80° F.

Augmented thrust. - The jet thrust of the installation was determined from the balance-scale measurements by the following equation:

$$F_{j,s} = B + D + D_r + \frac{W_{a,1}V_1}{g} + A_x(p_1 - p_0) \qquad (8)$$

The last two terms of this expression represent the momentum and pressure forces on the installation at the slip joint in the inlet-air duct. External drag of the installation was determined with the engine inoperative and the drag of the water-cooled exhaust-nozzle survey rake was measured by an air-balance piston mechanism.

Scale net thrust was obtained by subtracting the equivalent free-stream momentum of the inlet air from the scale jet thrust.

$$F_{n,s} = F_{j,s} - \frac{W_{a,1}V_0}{g} \qquad (9)$$

Normal engine thrust. - Normal engine thrust is the theoretical thrust that would be obtained with the engine and a standard engine tail pipe equipped with a nozzle of a size that gives the same turbine-outlet pressures and temperatures as were encountered with afterburning under the same flight conditions. The normal thrust of the engine was calculated from measurements during the afterburning program of total pressure and temperature at the turbine outlet and gas flow at the turbine outlet and also from previously determined total-pressure loss across the standard tail pipe.

$$F_{n,e} = C_V\left[\frac{W_{g,5}}{g}V_n + A_n(P_n - P_0)\right] - \frac{W_{a,1}V_0}{g} \qquad (10)$$

A value of unity was assumed for the velocity coefficient C_V used in equation (10). Experimental data indicated that the total-pressure loss through the standard tail pipe was approximately 0.01 P_5 at rated engine speed.

Augmented net-thrust ratio is defined as:

$$\frac{\text{Scale net thrust, } F_{n,s}}{\text{Normal engine net thrust, } F_{n,e}} \qquad (11)$$

REFERENCES

1. Jansen, Emmert T., and Thorman, H. Carl: Altitude Performance Characteristics of Tail-Pipe Burner with Variable-Area Exhaust Nozzle. NACA RM E50E29, 1950.

2. Conrad, E. William, and Prince, William R.: Altitude Performance and Operational Characteristics of 29-Inch-Diameter Tail-Pipe Burner with Several Fuel Systems and Flame Holders on J35 Turbojet Engine. NACA RM E9G08, 1949.

3. Conrad, E. William, and Jansen, Emmert T.: Effects of Internal Configurations on Afterburner Shell Temperatures. NACA RM E51I07, 1951.

4. Fleming, W. A., Conrad, E. William, and Young, A. W.: Experimental Investigation of Tail-Pipe-Burner Design Variables. NACA RM E50K22, 1951.

5. Wood, Charles C.: Preliminary Investigation of the Effects of Rectangular Vortex Generators on the Performance of a Short 1.9:1 Straight-Wall Annular Diffuser. NACA RM L51G09, 1951.

6. Mulready, Richard C.: The Ideal Temperature Rise Due to the Constant Pressure Combustion of Hydrocarbon Fuels. Meteor Rep. UAC-9, Res. Dept., United Aircraft Corp., July 1947. (Proj. Meteor, Bur. Ordnance Contract NOrd 9845 with M.I.T.)

7. Barson, Zelmar, and Sargent, Arthur F.: Effect of Fuel Volatility on Performance of Tail-Pipe Burner. NACA RM E51C14, 1951.

8. Nicholson, H. M., and Radcliffe, A.: Investigation of Pressure Fluctuations on a Derwent V Jet Engine. Rep. No. R-85, British N.G.T.E., Feb. 1951.

9. Fenn, J. B., Forney, H. B., and Garmon, R. C.: Burners for Supersonic Ramjets. Bumblebee Ser. Rep. 119, Experiment, Inc., Jan. 1950. (Bur. Ordnance Contract NOrd 9756.)

10. Bennett, D. G.: Suppression of Radiations at High Temperatures by Means of Ceramic Coatings. Jour. Am. Ceramic Soc., vol. 30, no. 10, Oct. 1, 1947, pp. 297-305.

11. Pinkel, Benjamin, and Turner, L. Richard: Thermodynamic Data for the Computation of the Performance of Exhaust-Gas Turbines. NACA ARR 4B25, 1944.

12. Wallner, Lewis E., and Wintler, John T.: Experimental Investigation of Typical Constant- and Variable-Area Exhaust Nozzles and Effects on Axial-Flow Turbojet-Engine Performance. NACA RM E51D19, 1951.

13. Turner, L. Richard, and Lord, Albert M.: Thermodynamic Charts for the Computation of Combustion and Mixture Temperatures at Constant Pressure. NACA TN 1086, 1946.

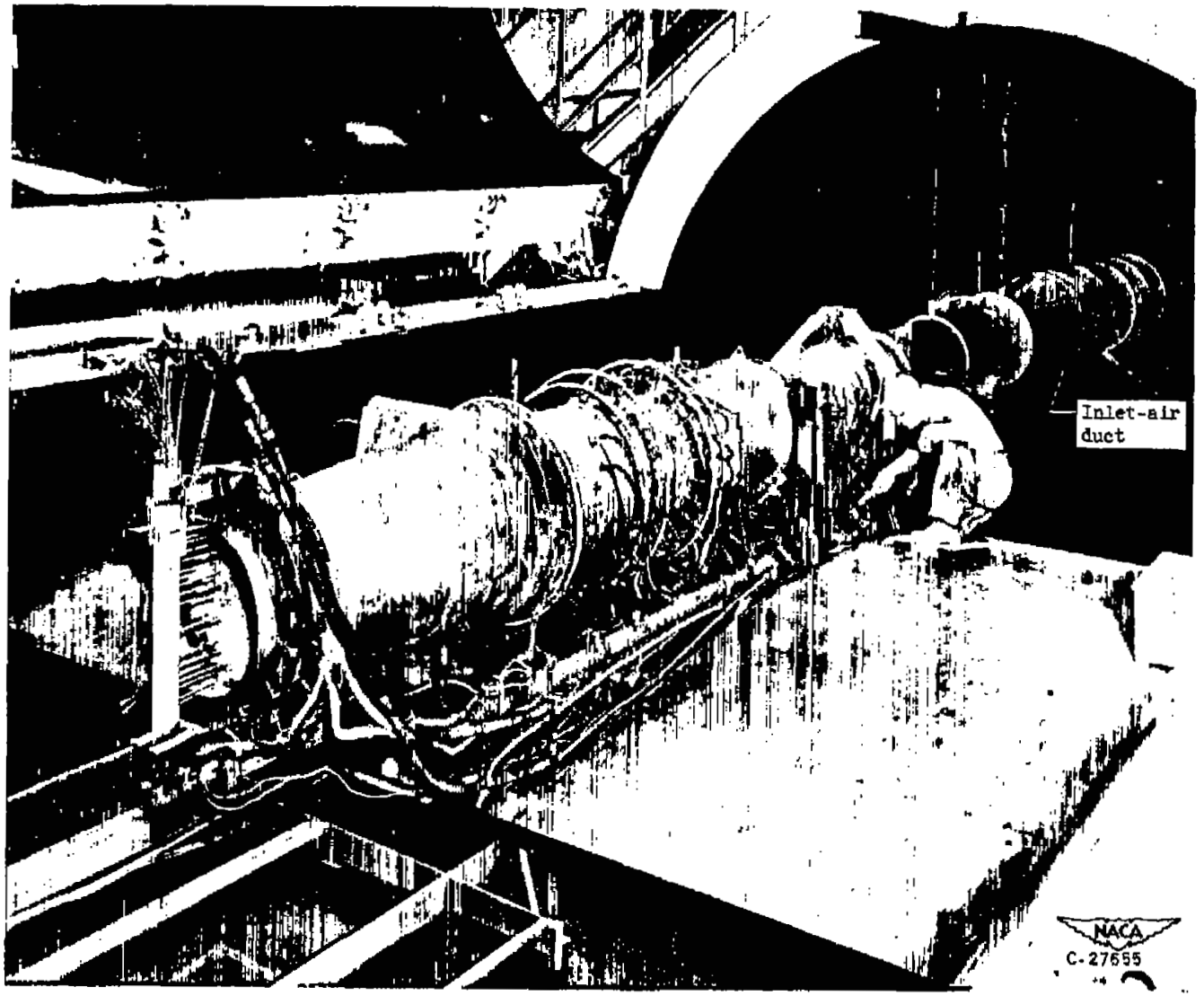

Figure 1. - Installation in test section of altitude wind tunnel.

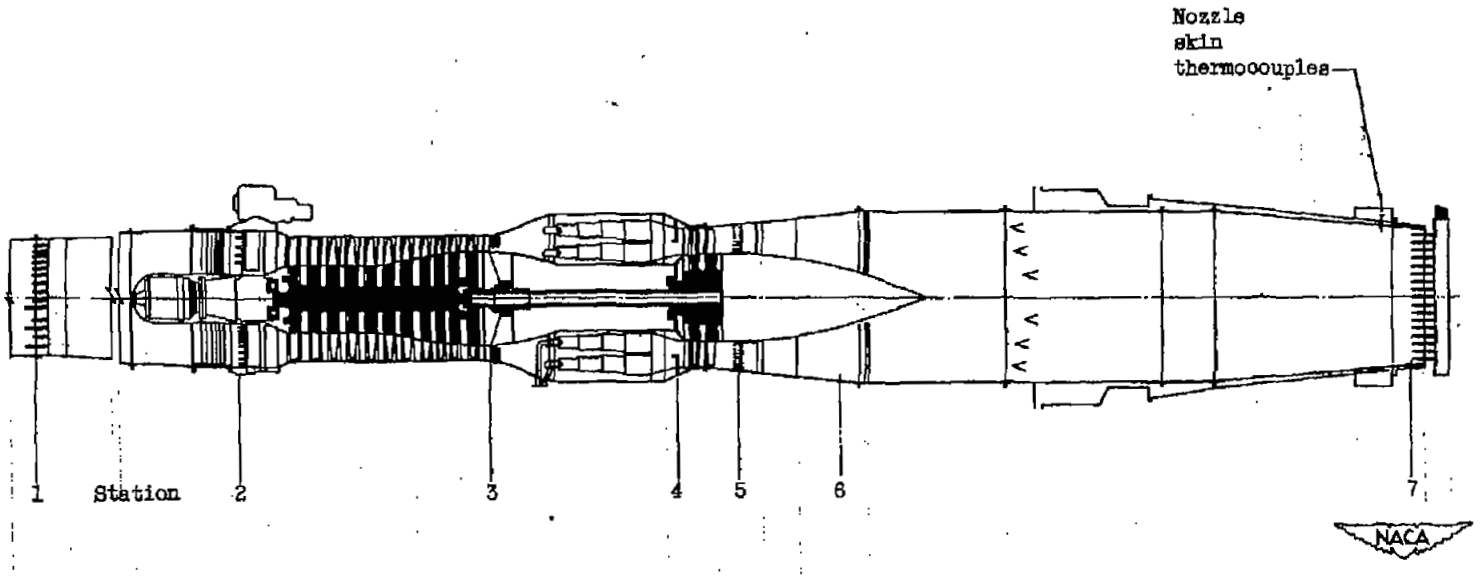

Station	1	2	3	4	5	6	7
Total-pressure tubes	17	16	10	5	21	8	12
Static-pressure tubes	3	8	6	-	--	-	5
Wall static orifices	4	4	4	-	3	1	4
Thermocouples	9	8	8	-	36	-	--

Figure 2. - View of engine showing location of stations at which instrumentation was installed.

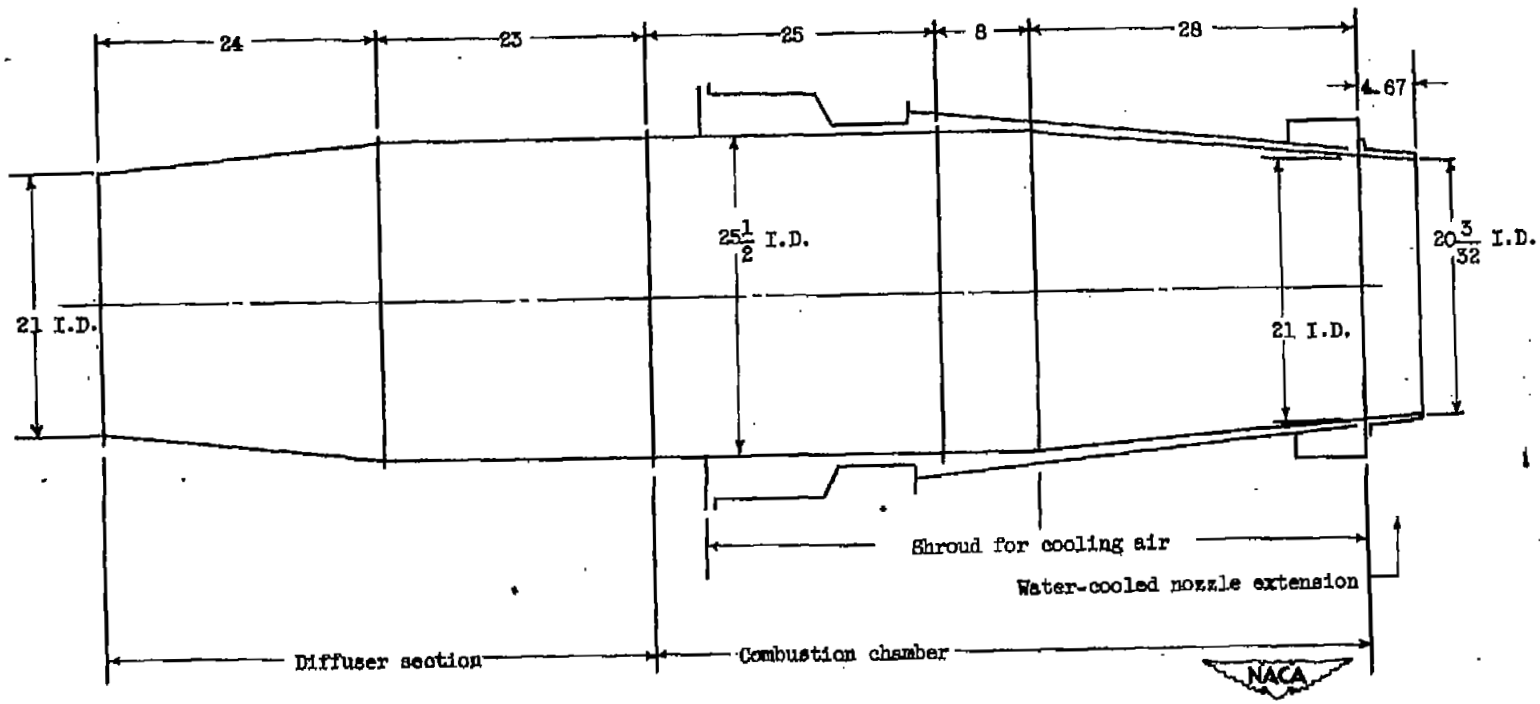

Figure 3. - Details of afterburner shell and external cooling shroud. (All dimensions in inches.)

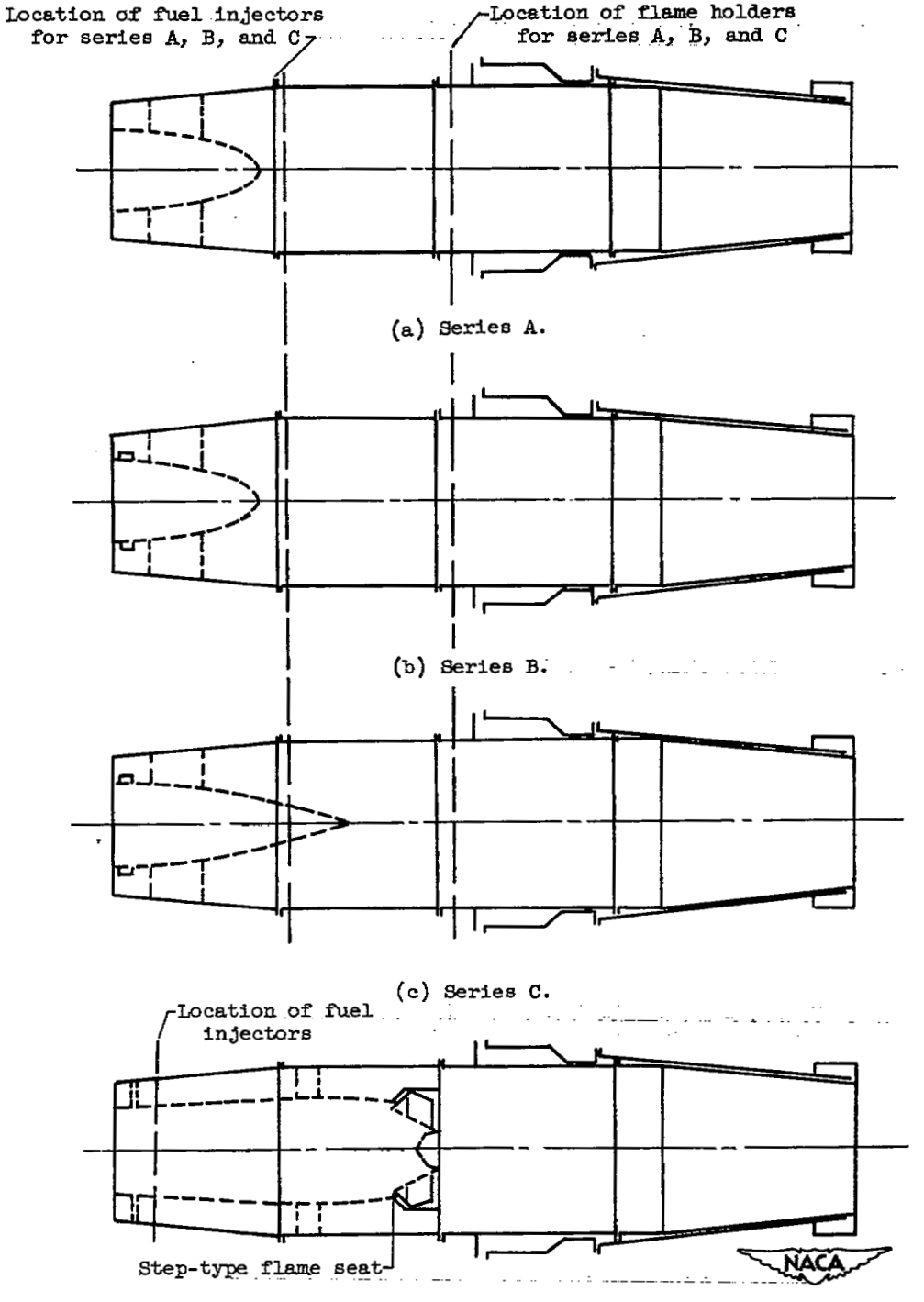

Figure 4. - Diffuser inner-cone modifications in four series of configurations.

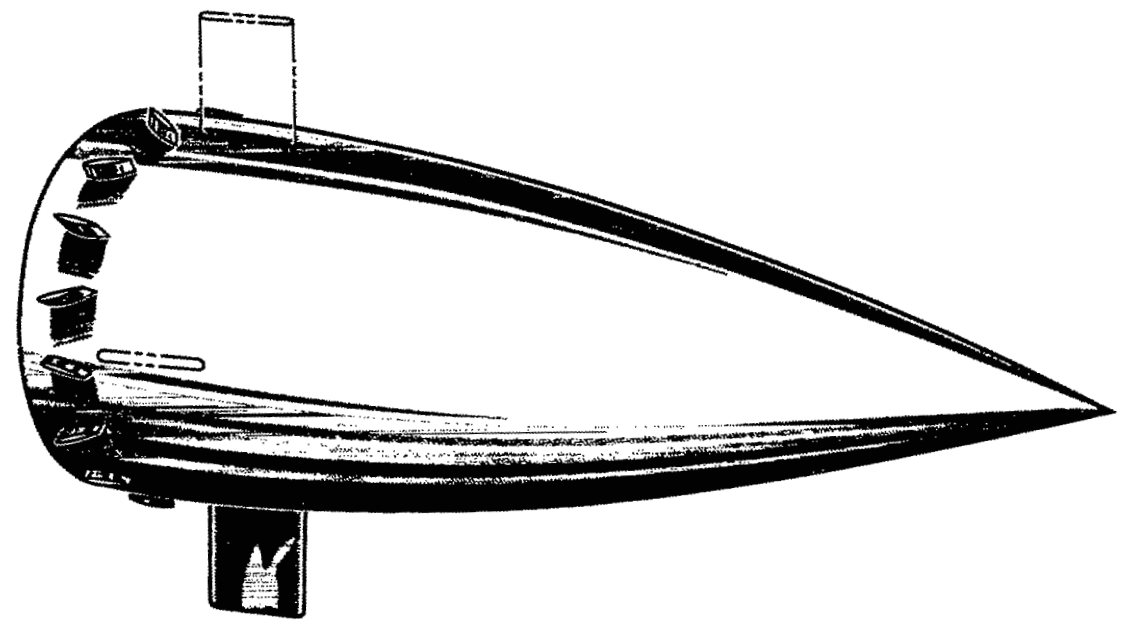

Figure 5. - Vortex generator installation for series C configurations.

[redacted]

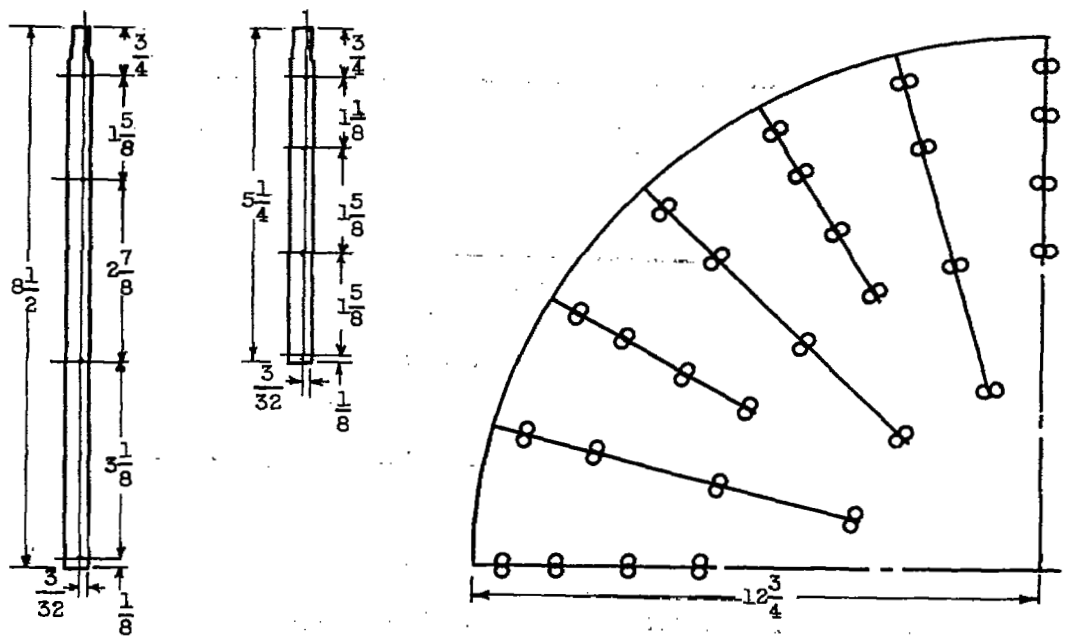

(a) Optimum pattern for series A. Diameter of all holes, 0.0225 inches.

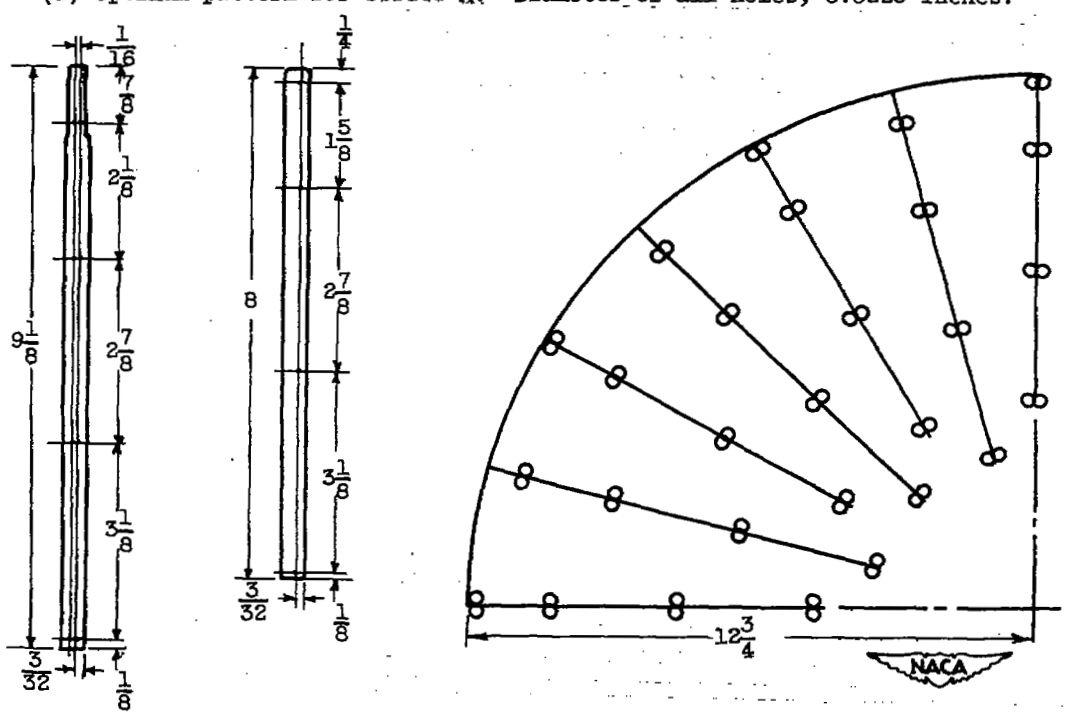

(b) Optinum pattern for series B. Diameter of all holes, 0.0225 inches.

Figure 6. - Details of optimum fuel-distribution patterns for series A, B, C, and D. (All dimensions in inches.)

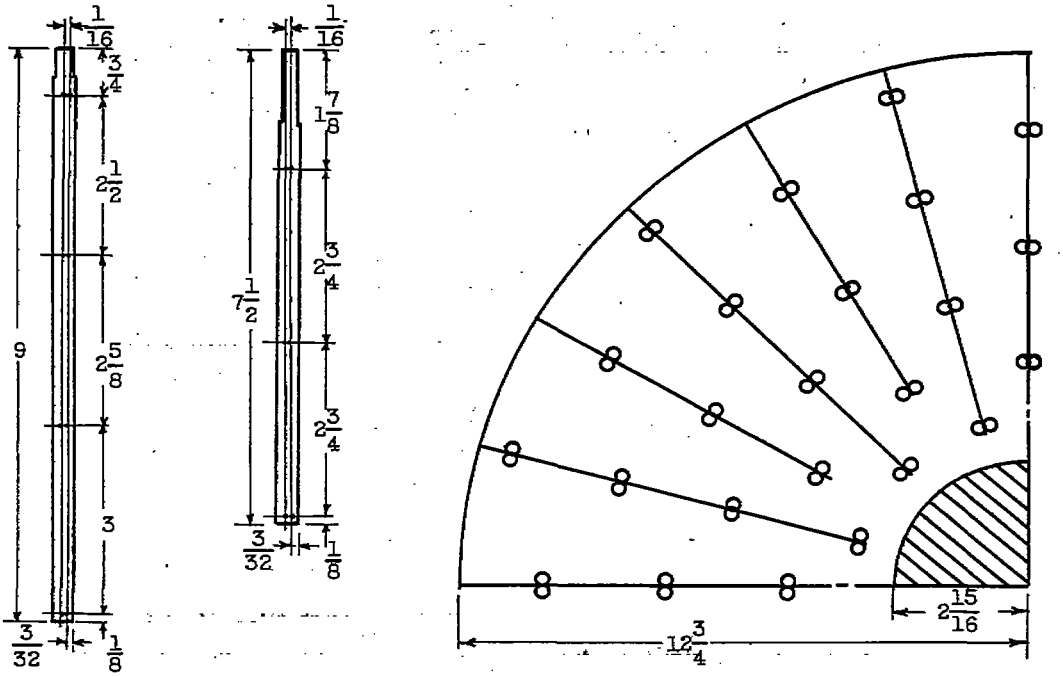

(c) Optimum pattern for series C. Diameter of all holes, 0.016 inches.

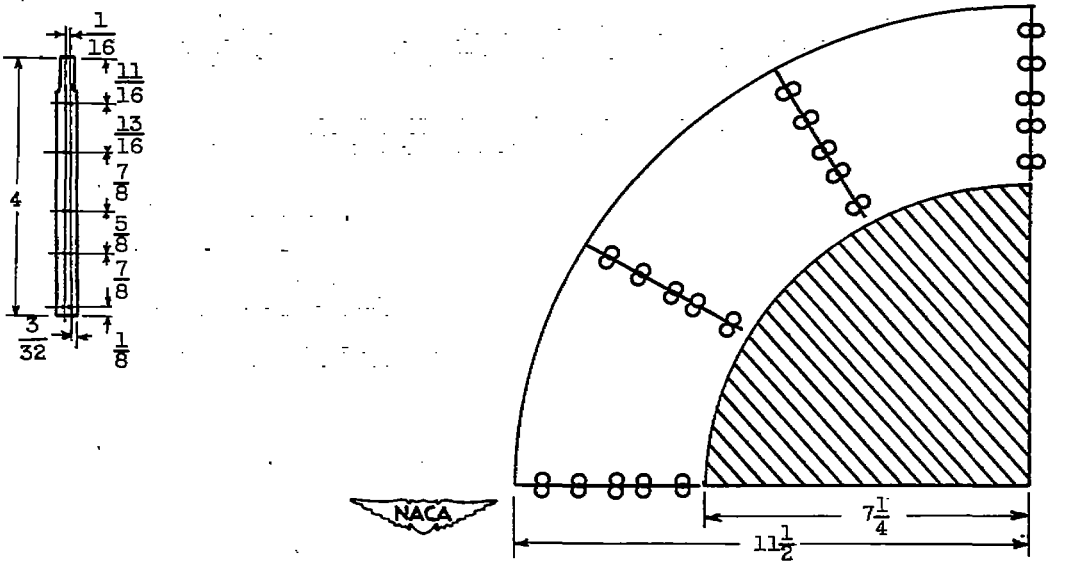

(d) Optimum pattern for series D. Diameter of all holes, 0.025 inches.

Figure 6. - Concluded. Details of optimum fuel-distribution patterns for series A, B, C, and D. (All dimensions in inches.)

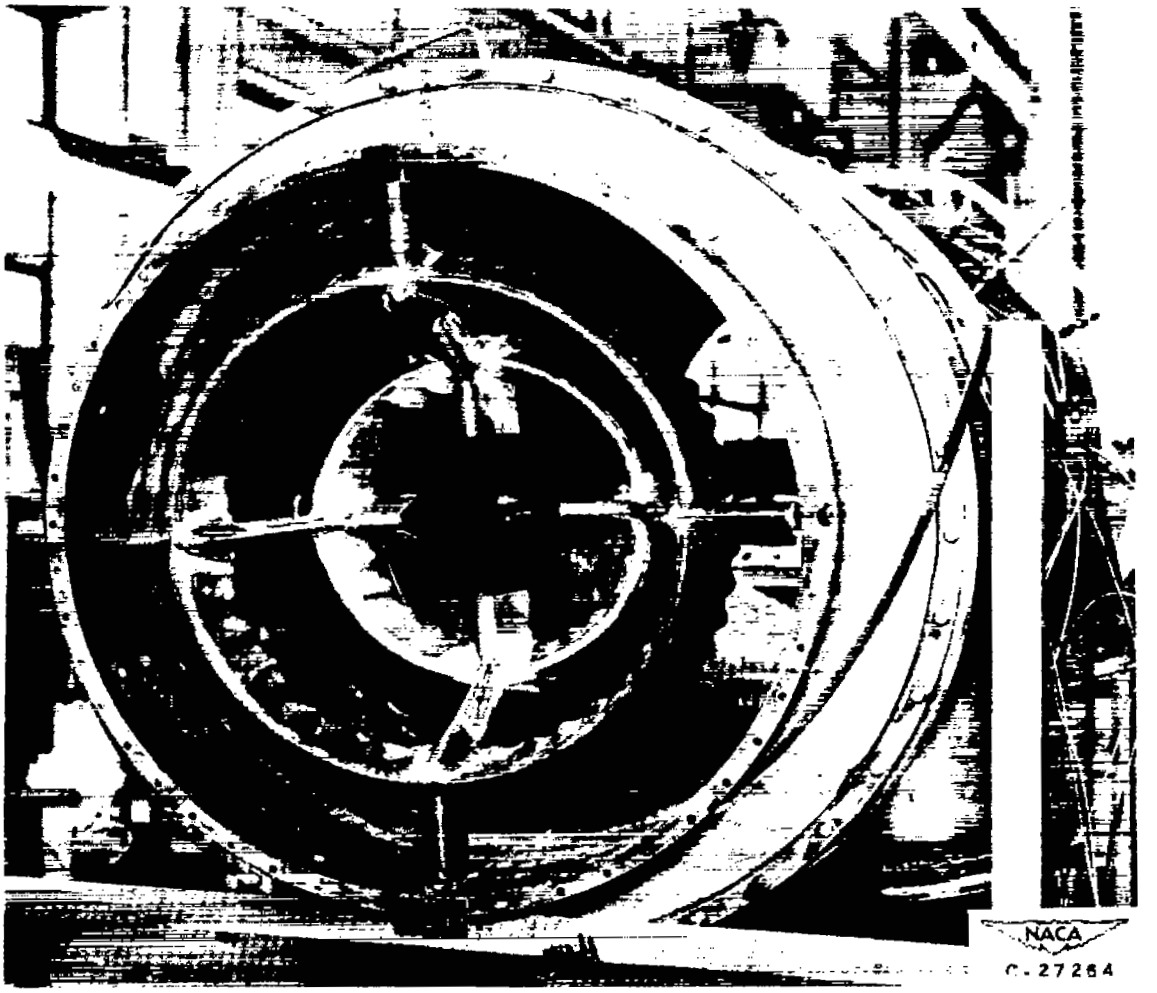

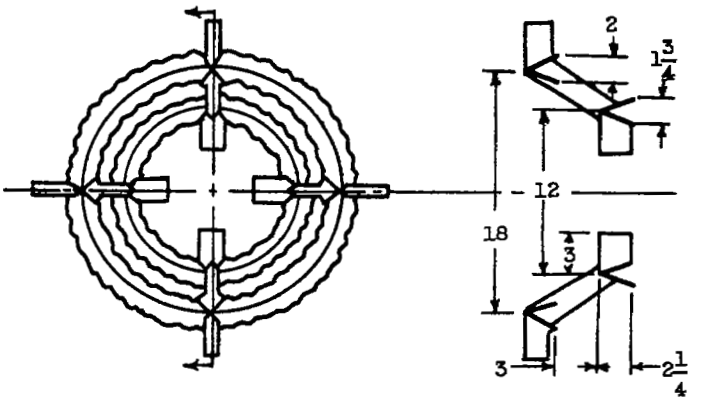

(a) Flame holder 1; blockage, 40 percent.

Figure 7. - Details of flame holders used on series A, B, and C. (All dimensions in inches.)

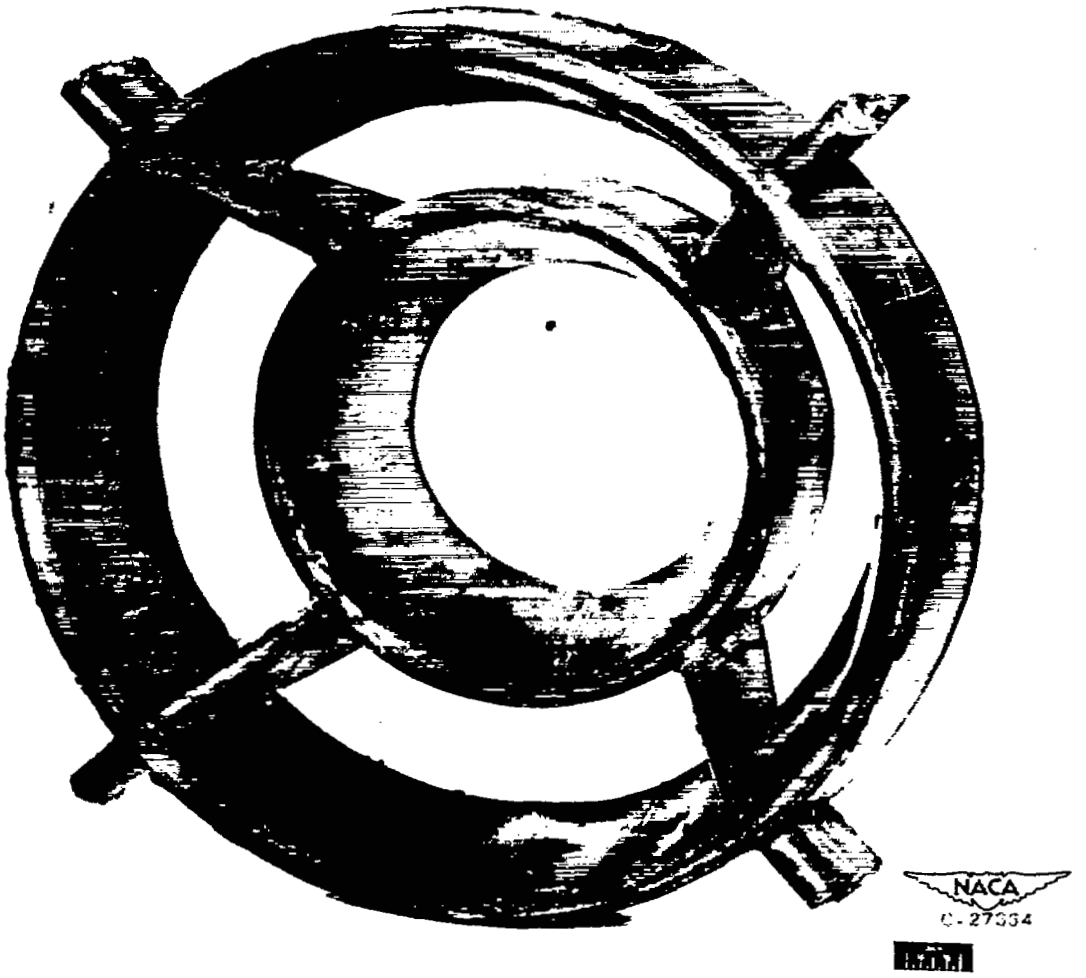

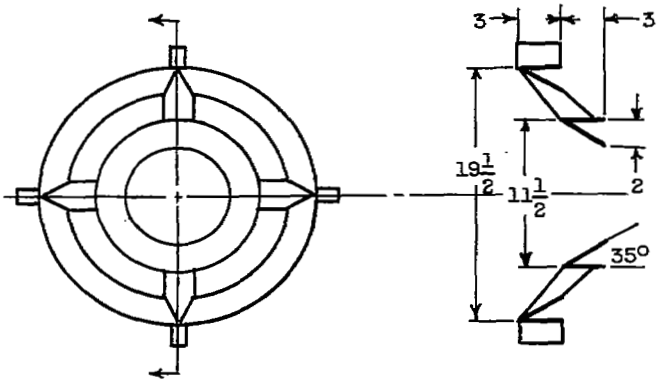

(b) Flame holder 2; blockage, 38 percent.

Figure 7. - Continued. Details of flame holders used on series A, B, and C. (All dimensions in inches.)

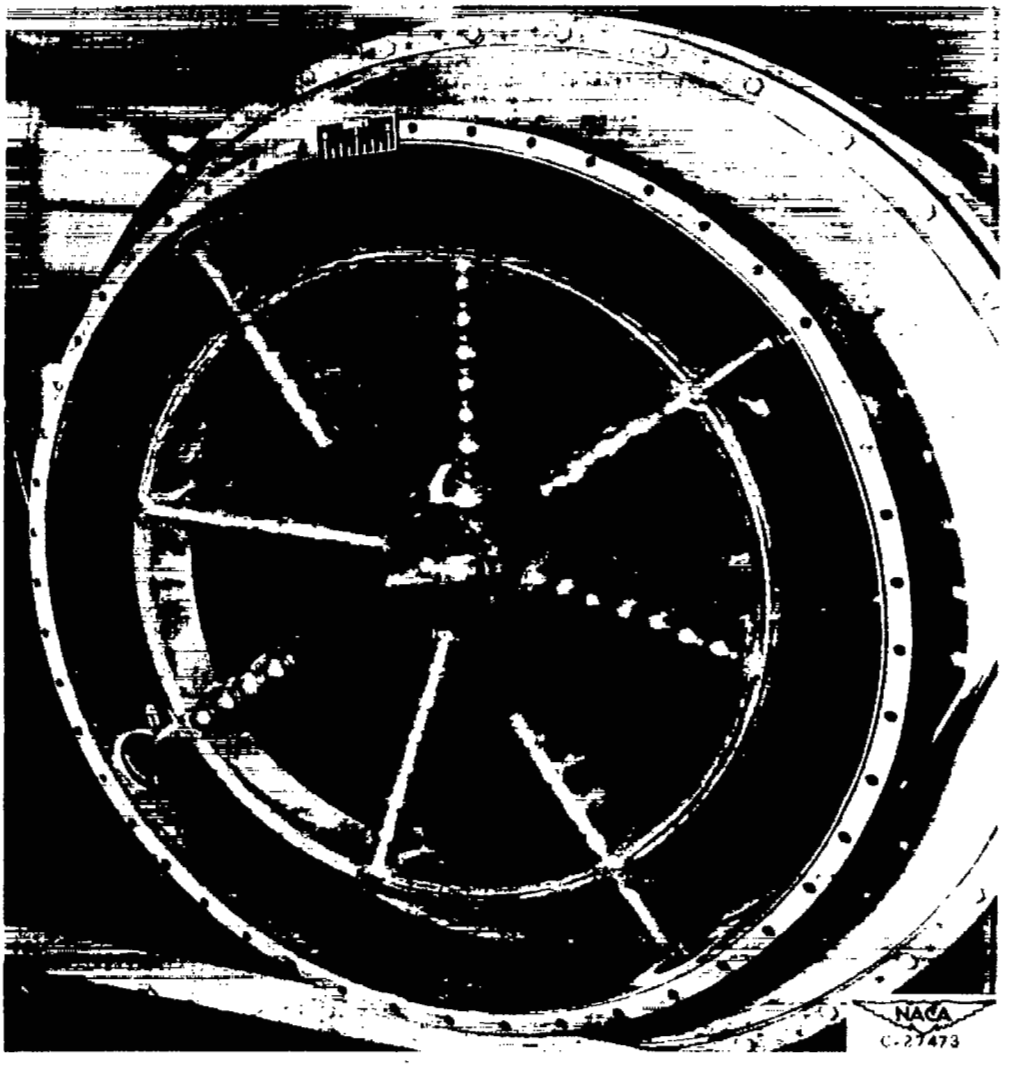

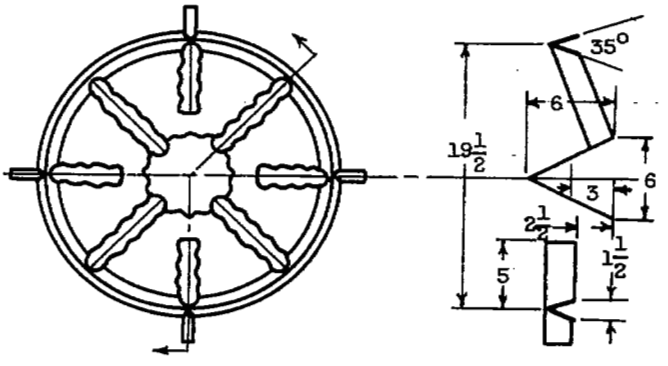

(c) Flame holder 3; blockage, .37 percent.

Figure 7. - Continued. Details of flame holders used on series A, B, and C. (All dimensions in inches.)

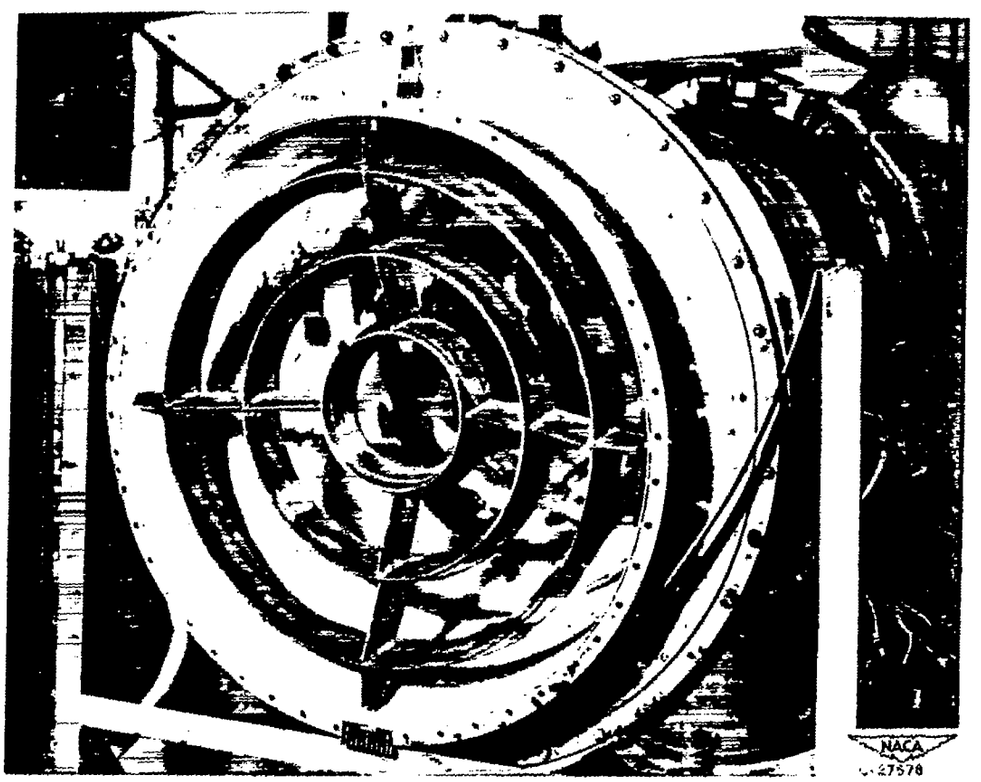

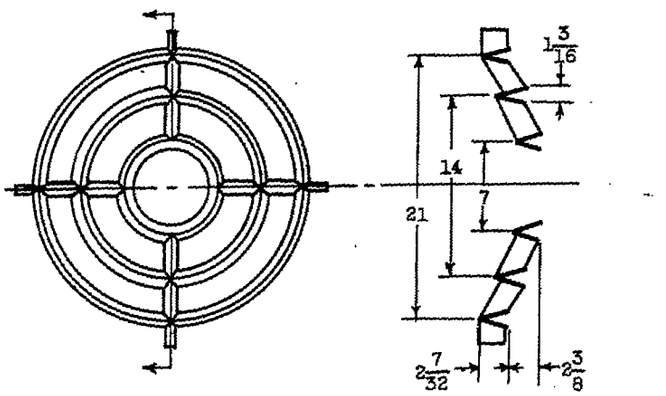

(d) Flame holder 4; blockage, 35 percent.

Figure 7. - Continued. Details of flame holders used on series A, B, and C. (All dimensions in inches.)

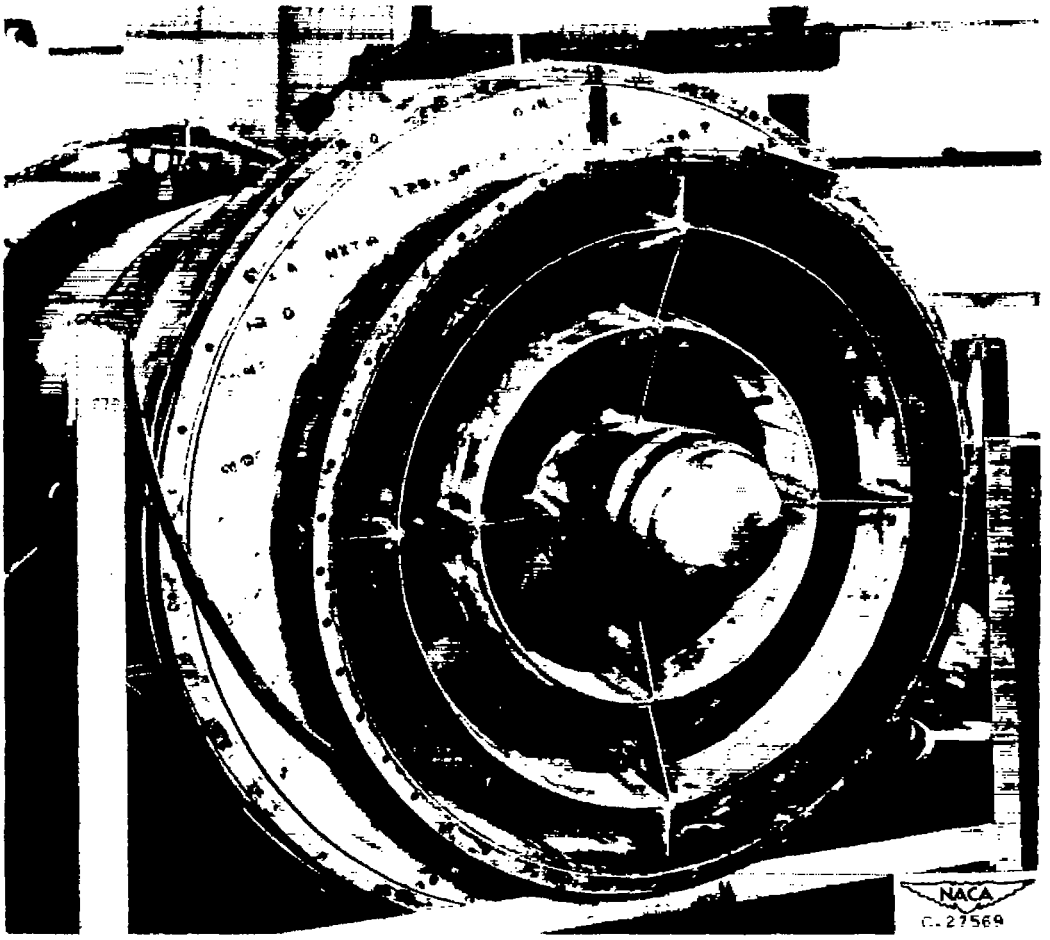

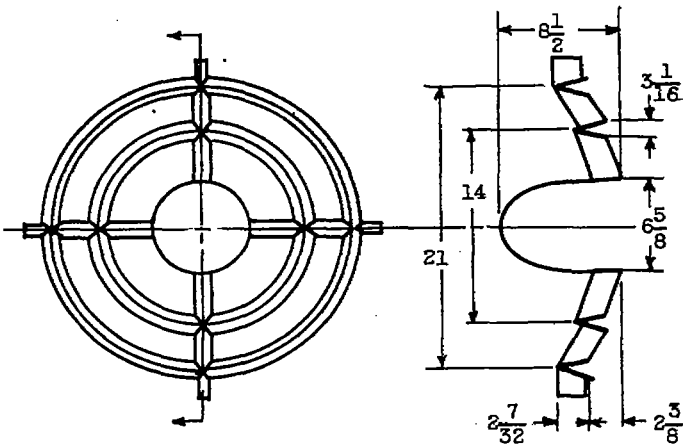

(e) Flame holder 5; blockage, 37 percent.

Figure 7. - Concluded. Details of flame holders used on series A, B, and C. (All dimensions in inches.)

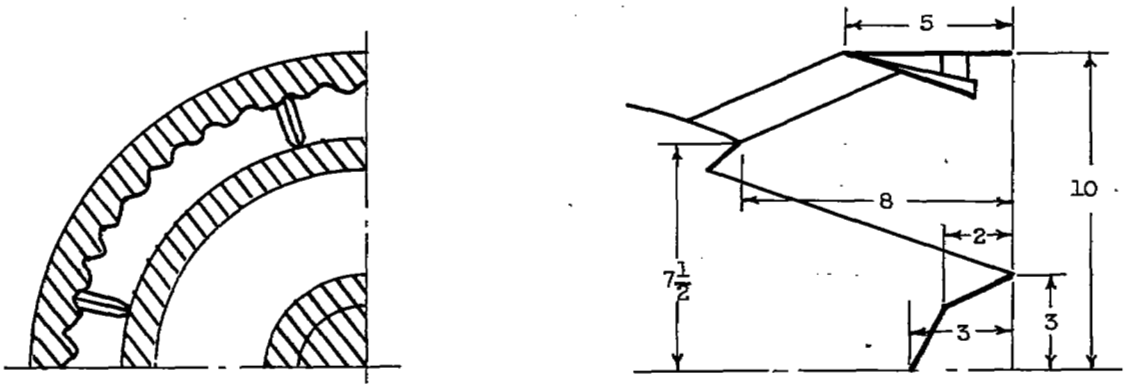

(a) Flame holder 6.

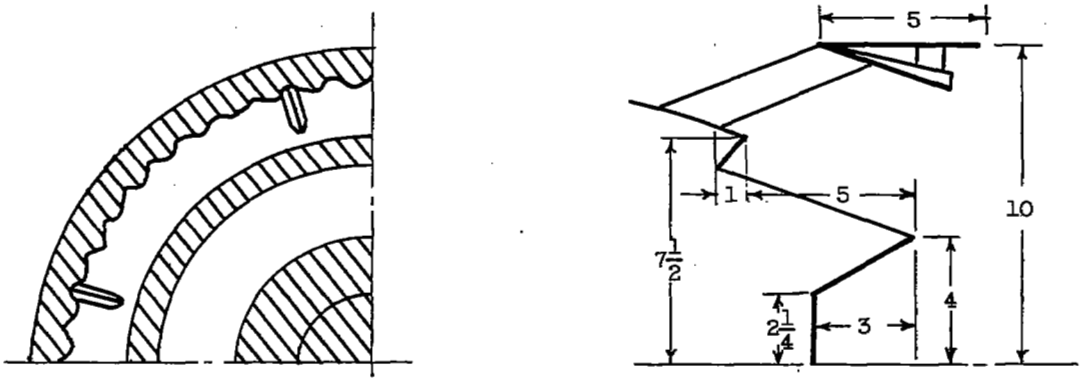

(b) Flame holder 7.

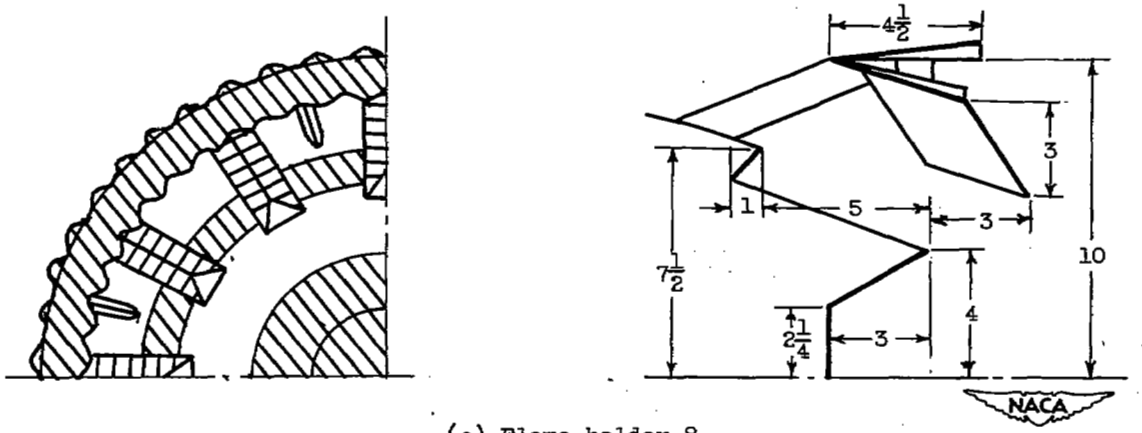

(c) Flame holder 8.

Figure 8. - Details of flame holders used with series D.
(All dimensions in inches.)

[redacted]

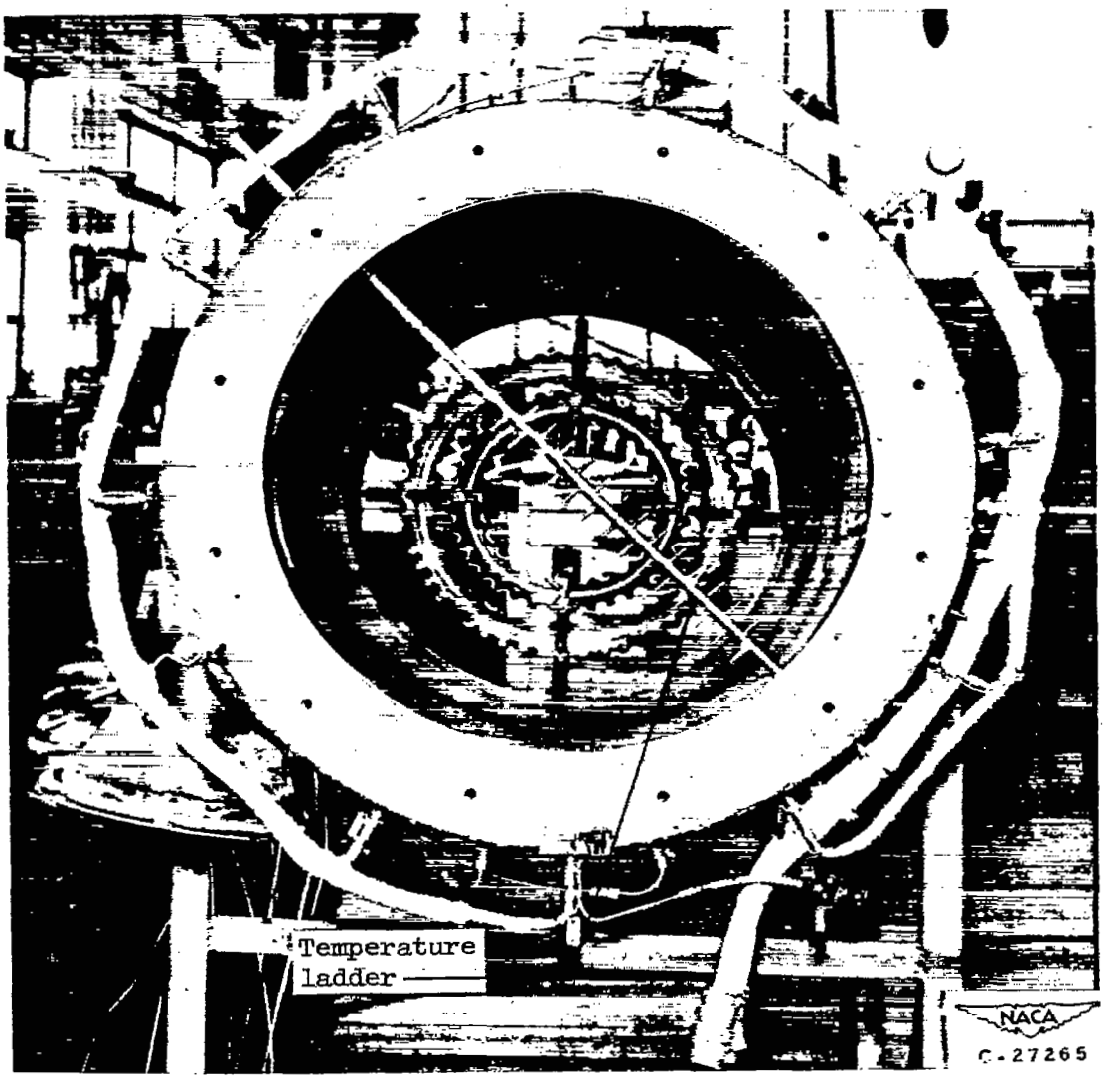

Figure 9. - Temperature ladder installed at exhaust-nozzle inlet.

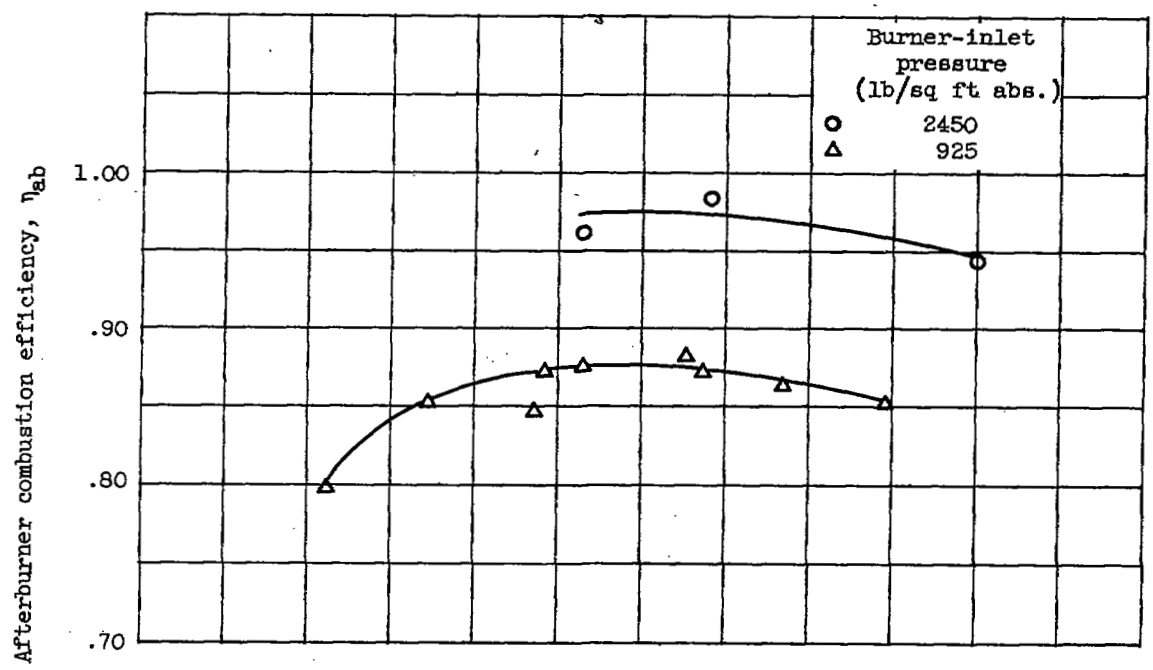

(a) Afterburner combustion efficiency.

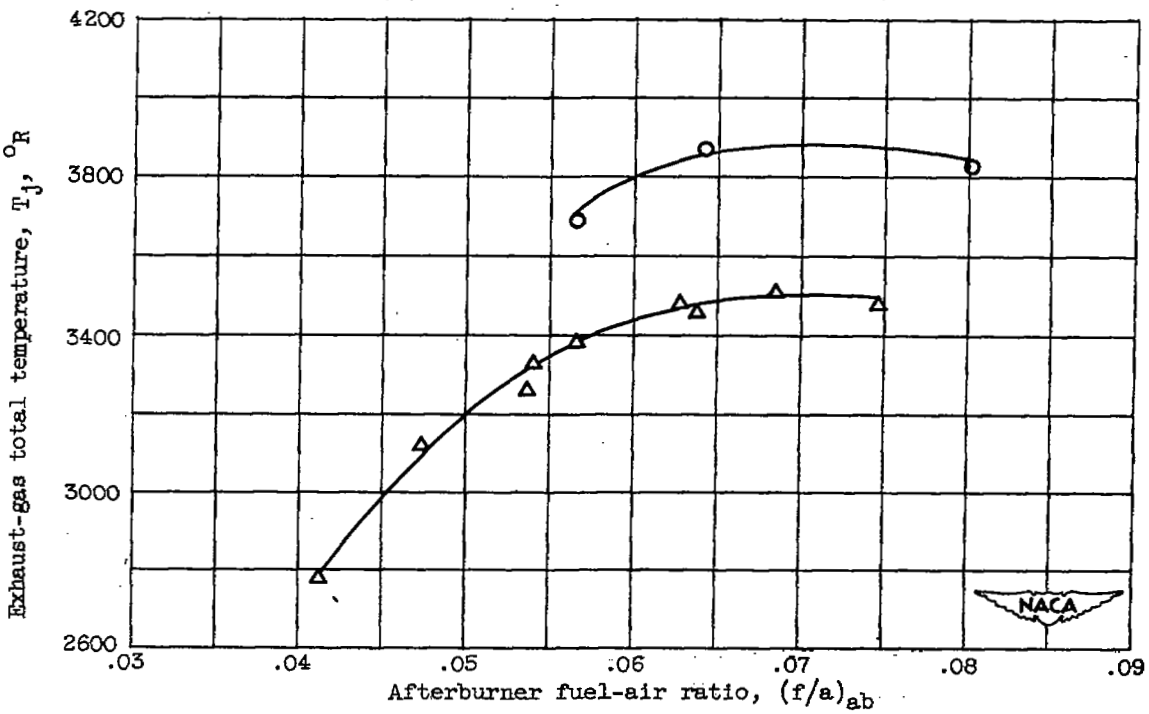

(b) Exhaust-gas total temperature.

Figure 10. - Performance obtained with best configuration in series A.

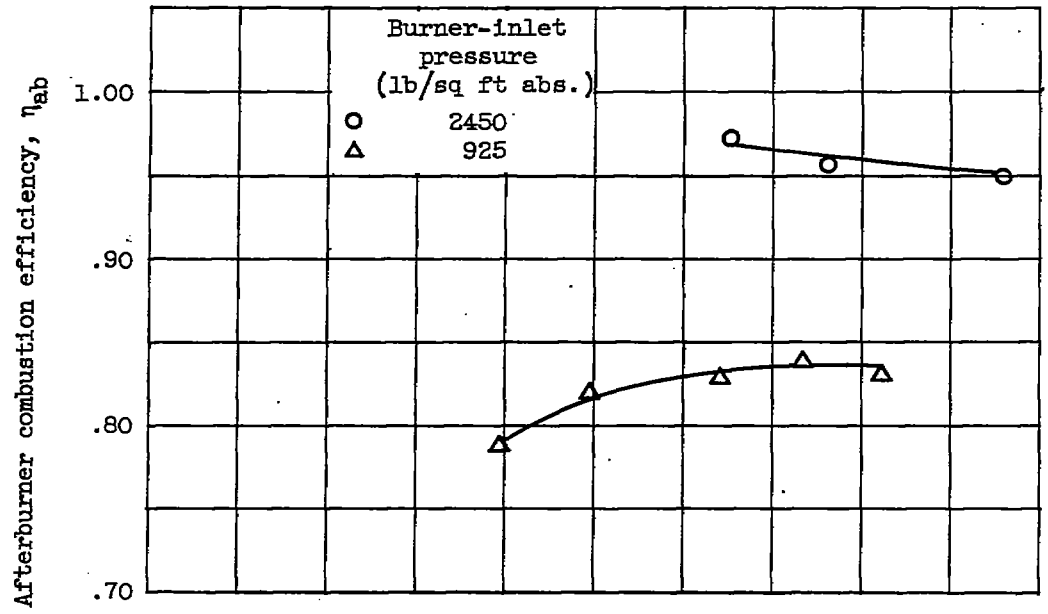

(a) Afterburner combustion efficiency.

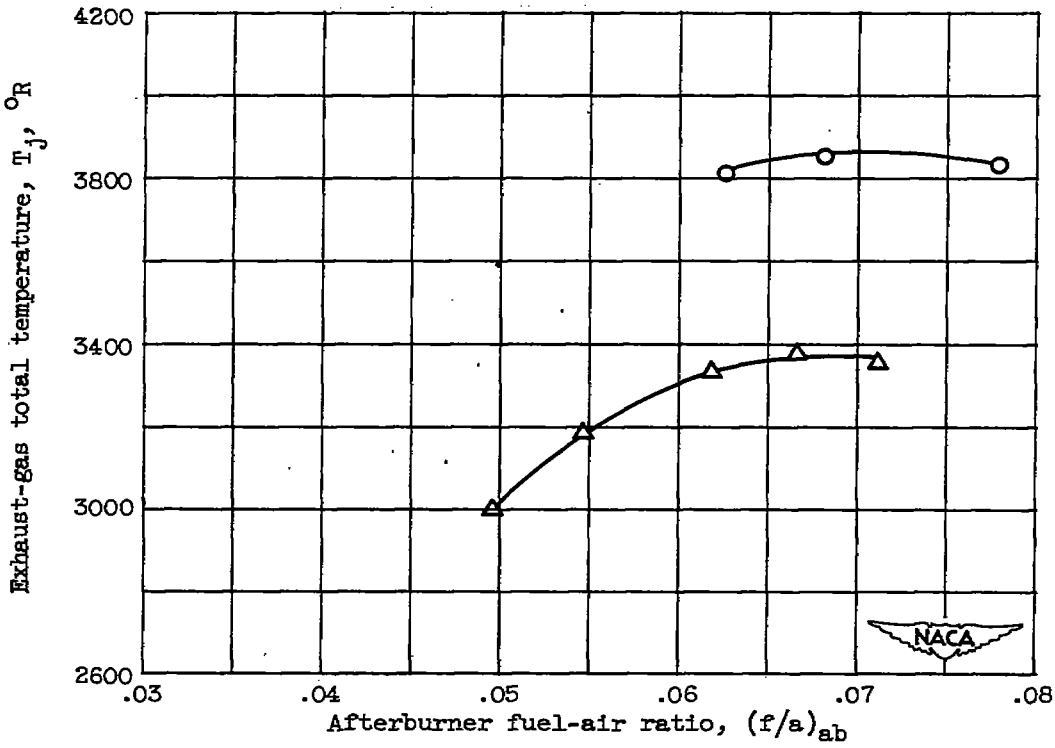

(b) Exhaust-gas total temperature.

Figure 11. - Performance obtained with best configuration in series B.

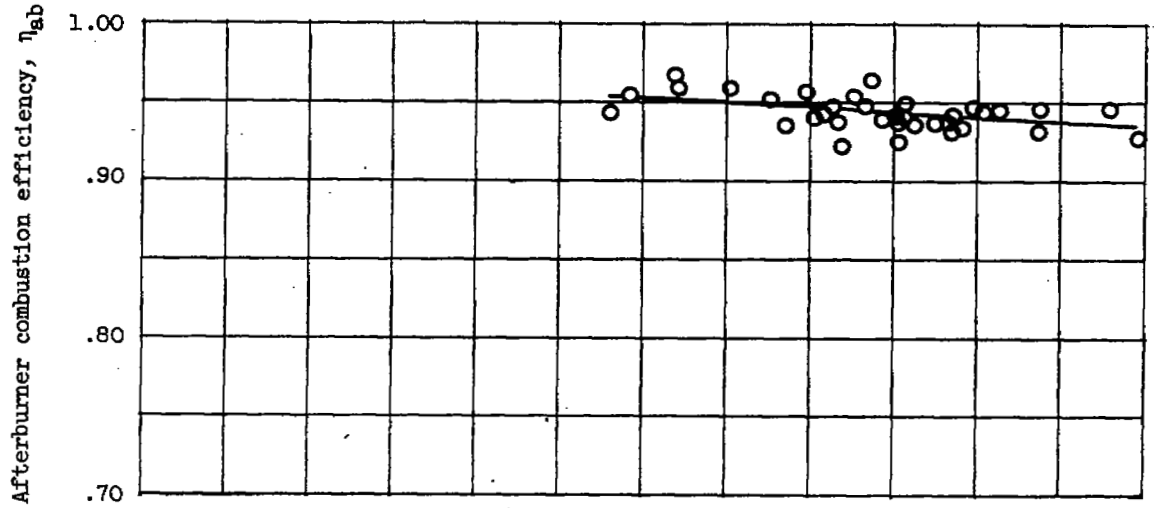

(a) Afterburner combustion efficiency.

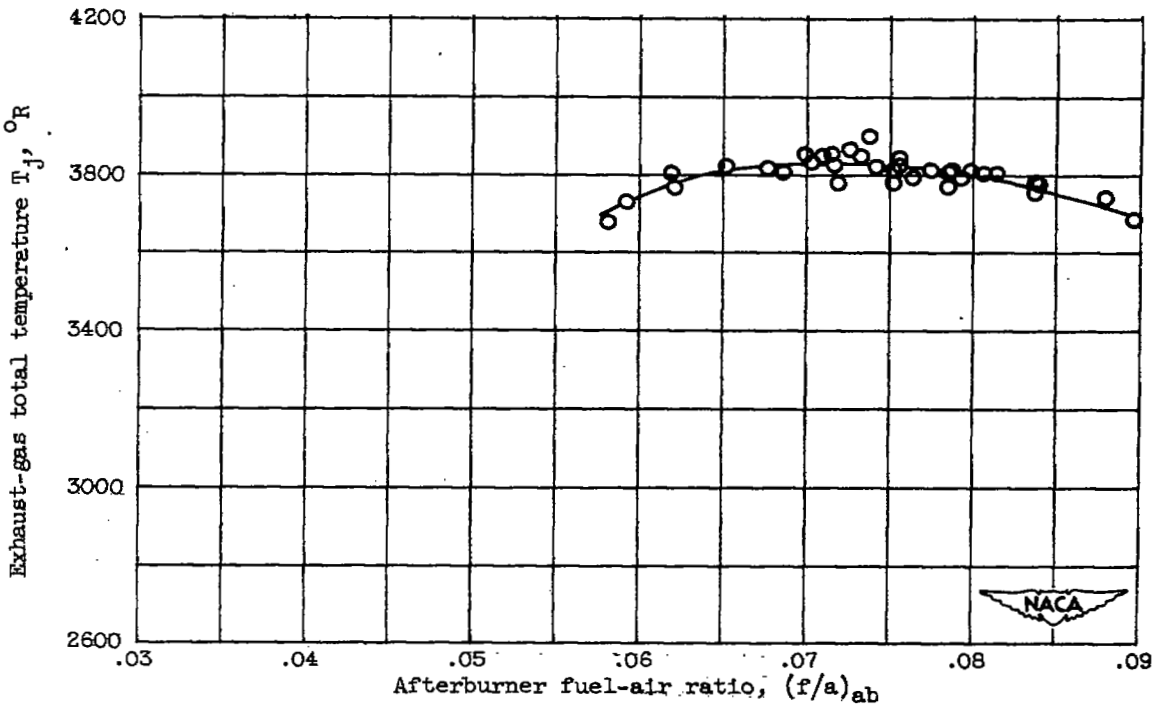

(b) Exhaust-gas total temperature.

Figure 12. - Performance obtained with best configuration in series C at burner-inlet pressure of 2450 pounds per square foot absolute.

[redacted]

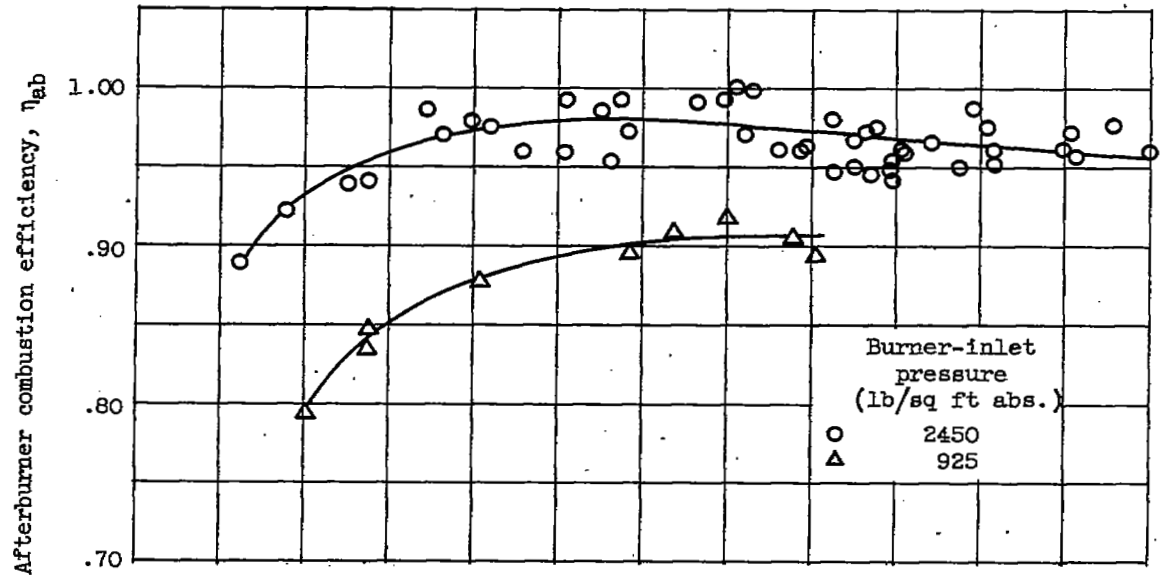

(a) Afterburner combustion efficiency.

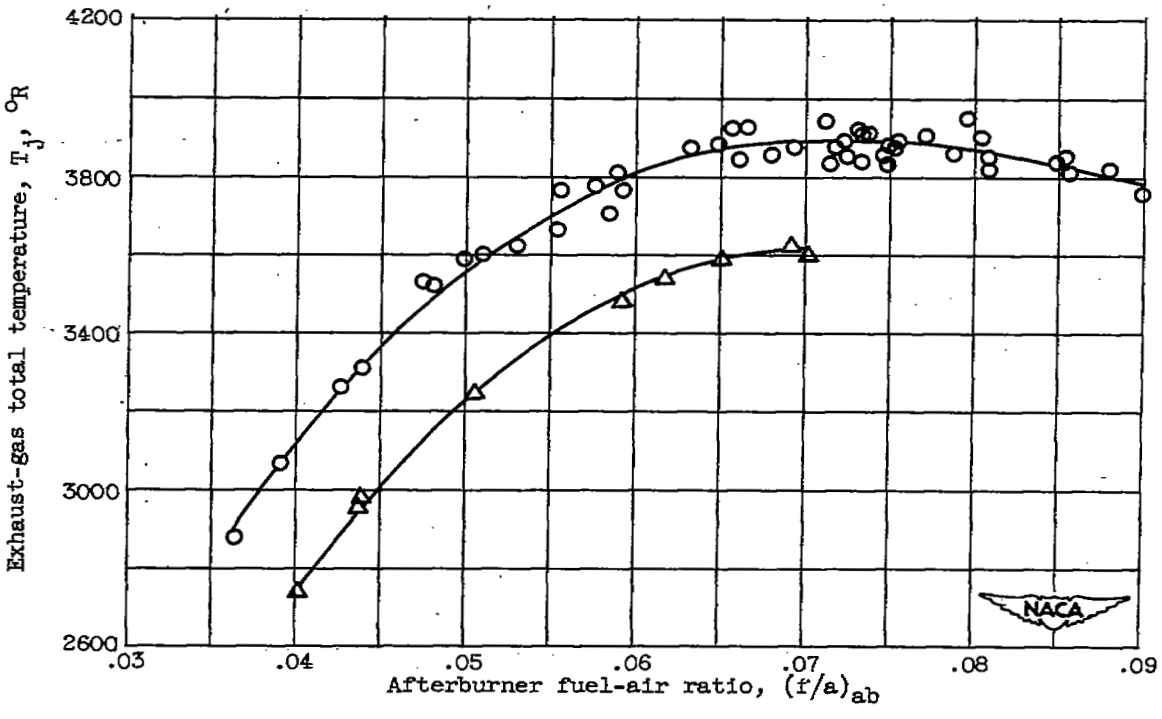

(b) Exhaust-gas total temperature.

Figure 13. - Performance obtained with best configuration in series D.

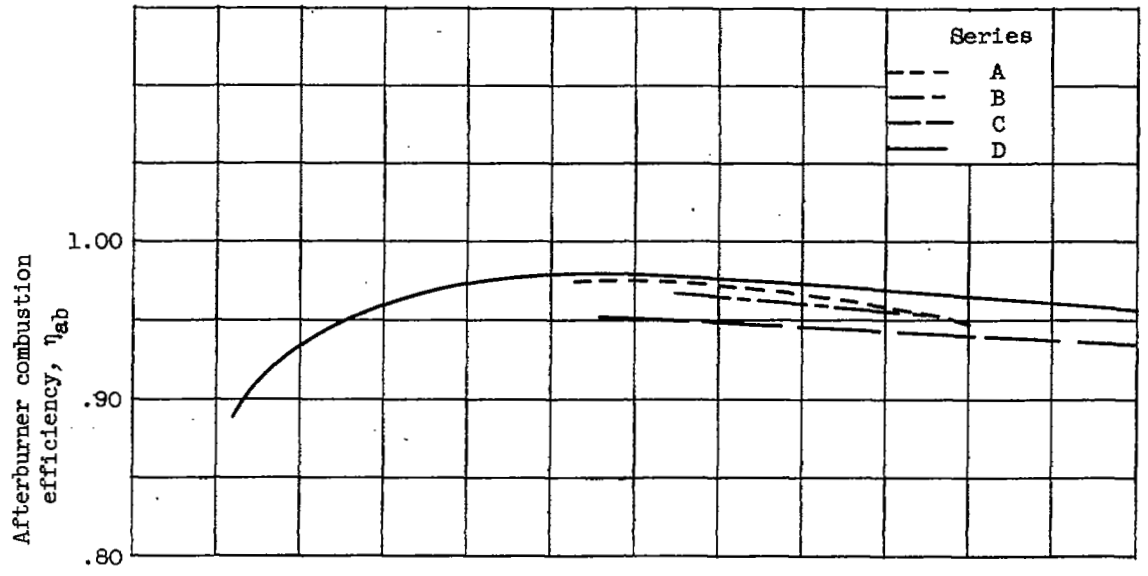

(a) Afterburner combustion efficiency.

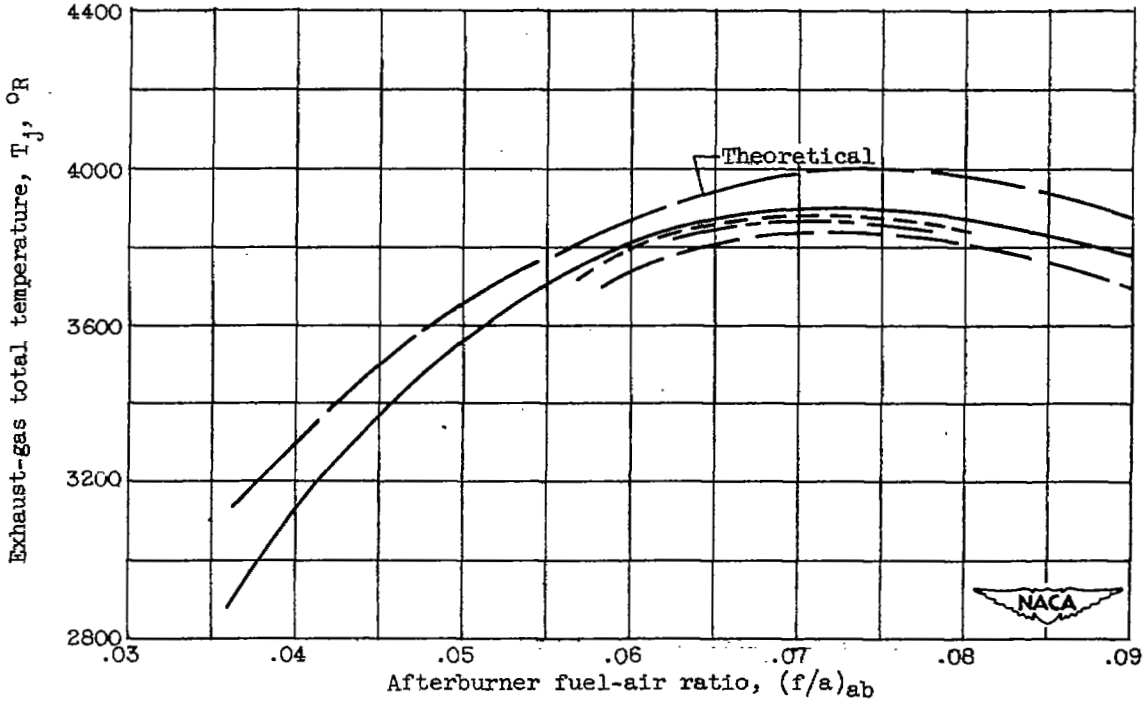

(b) Exhaust-gas total temperature.

Figure 14. - Performance obtained with best configurations in series A, B, C, and D at burner-inlet pressure of 2450 pounds per square foot absolute.

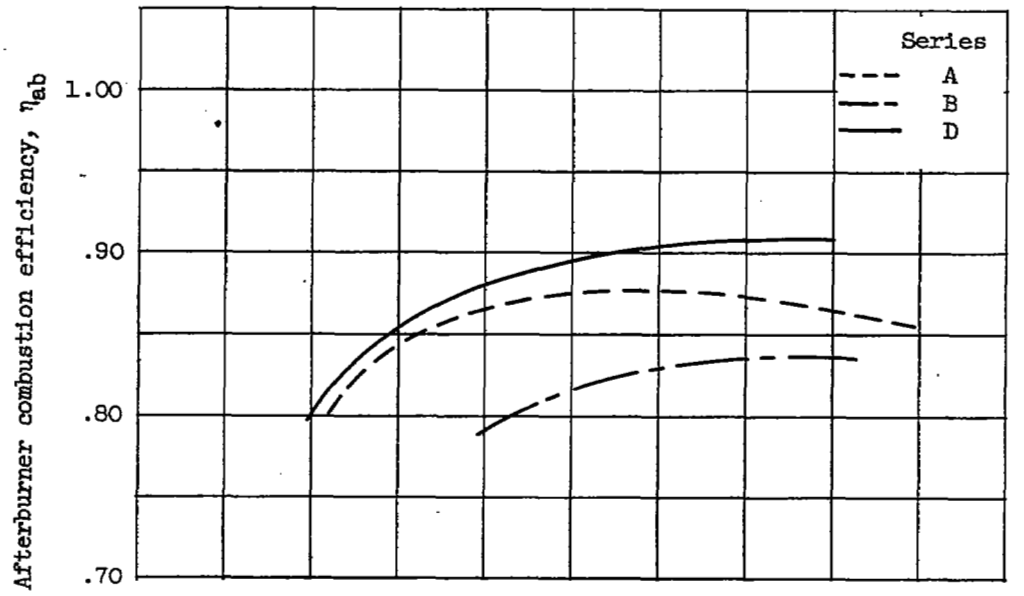

(a) Afterburner combustion efficiency.

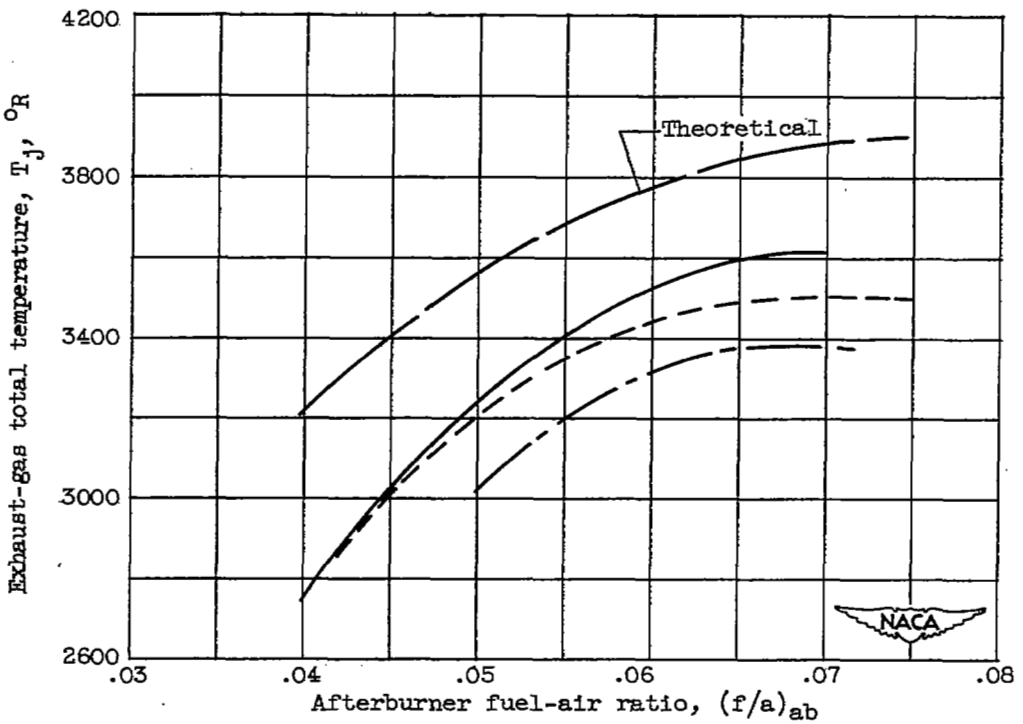

(b) Exhaust-gas total temperature.

Figure 15. - Performance obtained with best configurations in series A, B, and D at burner-inlet pressure of 925 pounds per square foot absolute.

[redacted]

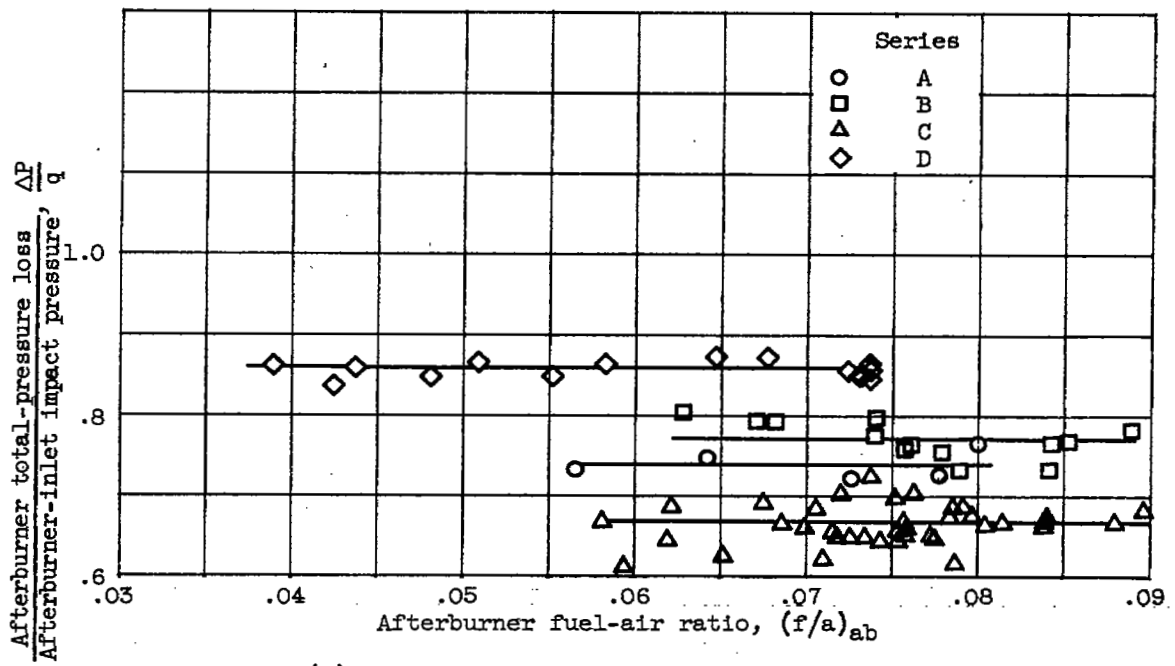

(a) Afterburner pressure-loss characteristics.

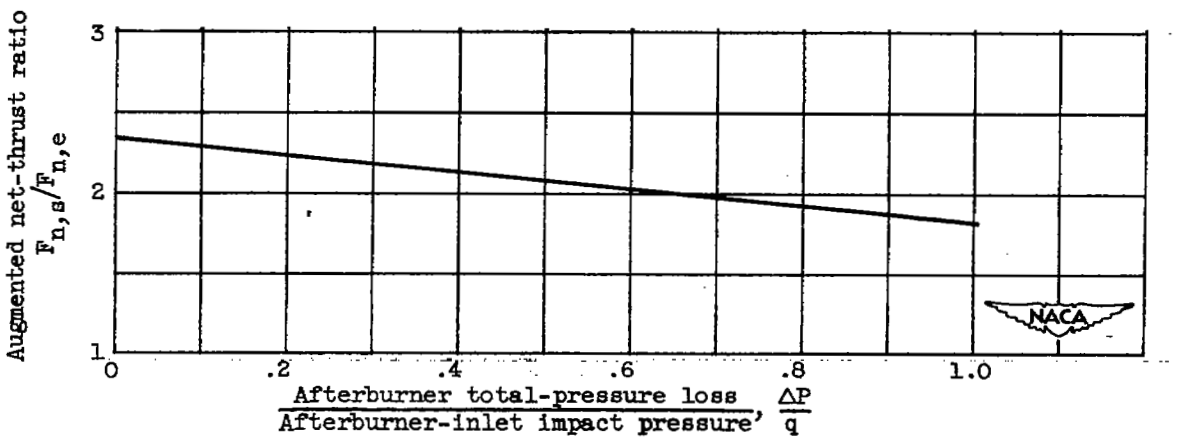

(b) Effect of afterburner pressure-loss characteristics on augmented thrust ratio; turbine-outlet temperature, 1660° R; exhaust-gas total temperature, 3900° R; altitude, 25,000 feet; flight Mach number, 0.92.

Figure 16. - Afterburner pressure-loss characteristics and effect on augmented net-thrust ratio.

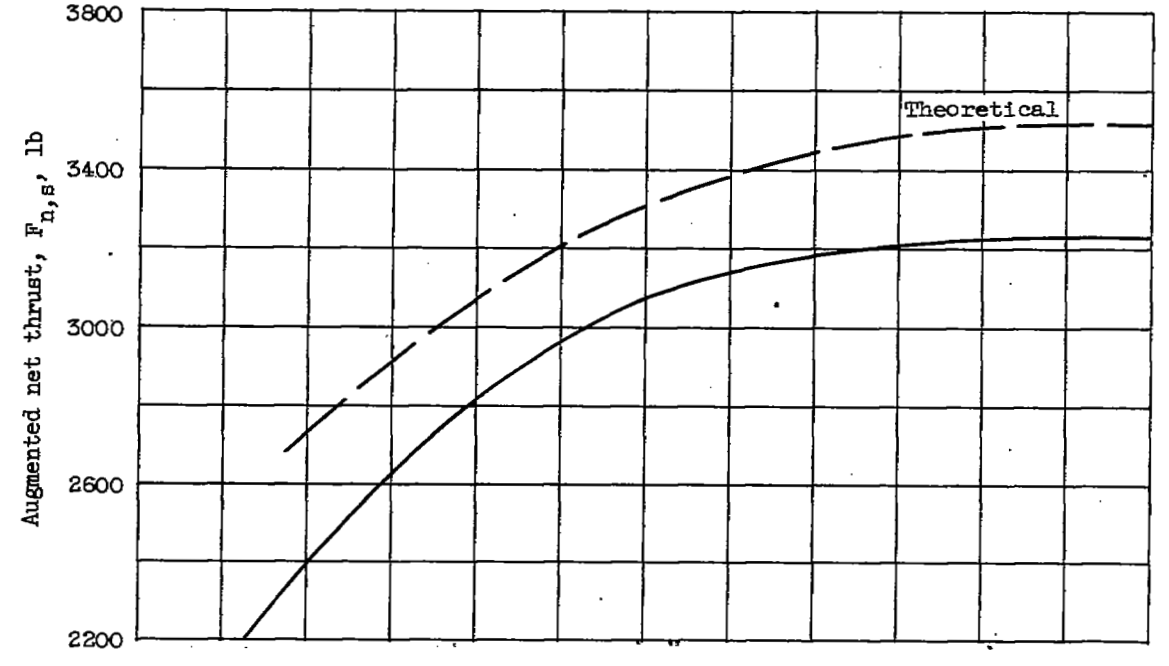

(a) Augmented net thrust.

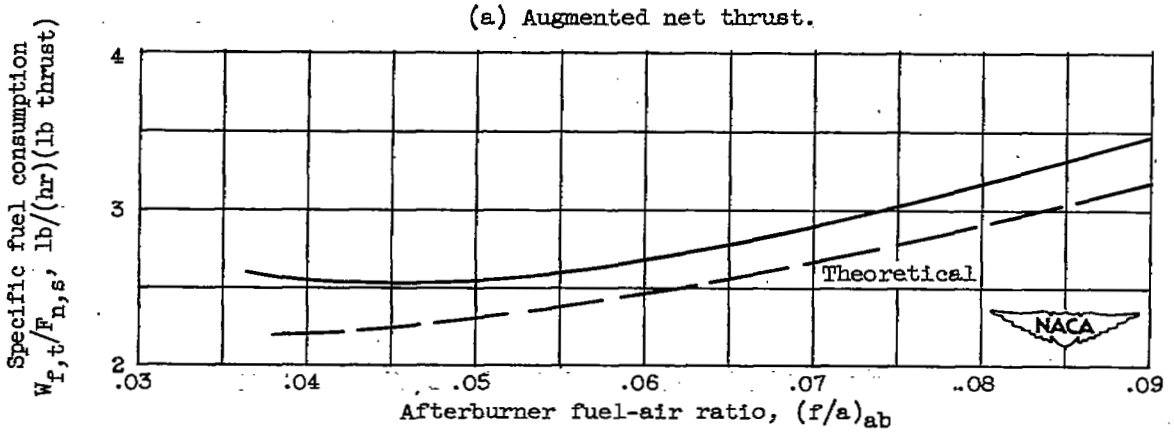

(b) Specific fuel consumption.

Figure 17. - Comparison of performance obtained with configuration D and performance theoretically possible at burner-inlet pressure of 2450 pounds per square foot absolute. Altitude, 25,000 feet; flight Mach number, 0.92.

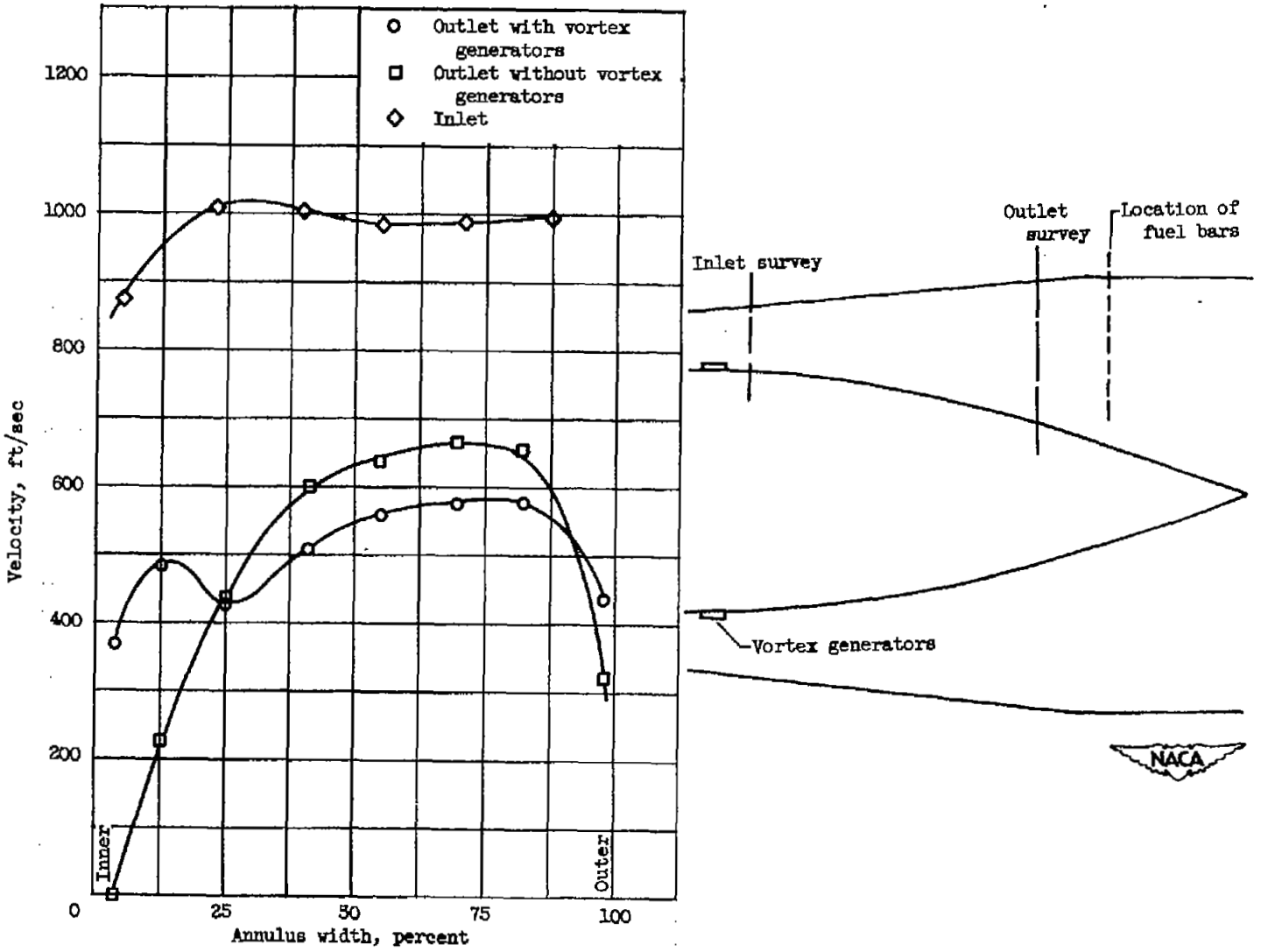

Figure 18. - Effect of vortex generators on diffuser-outlet velocity profiles. Series C inner cone.

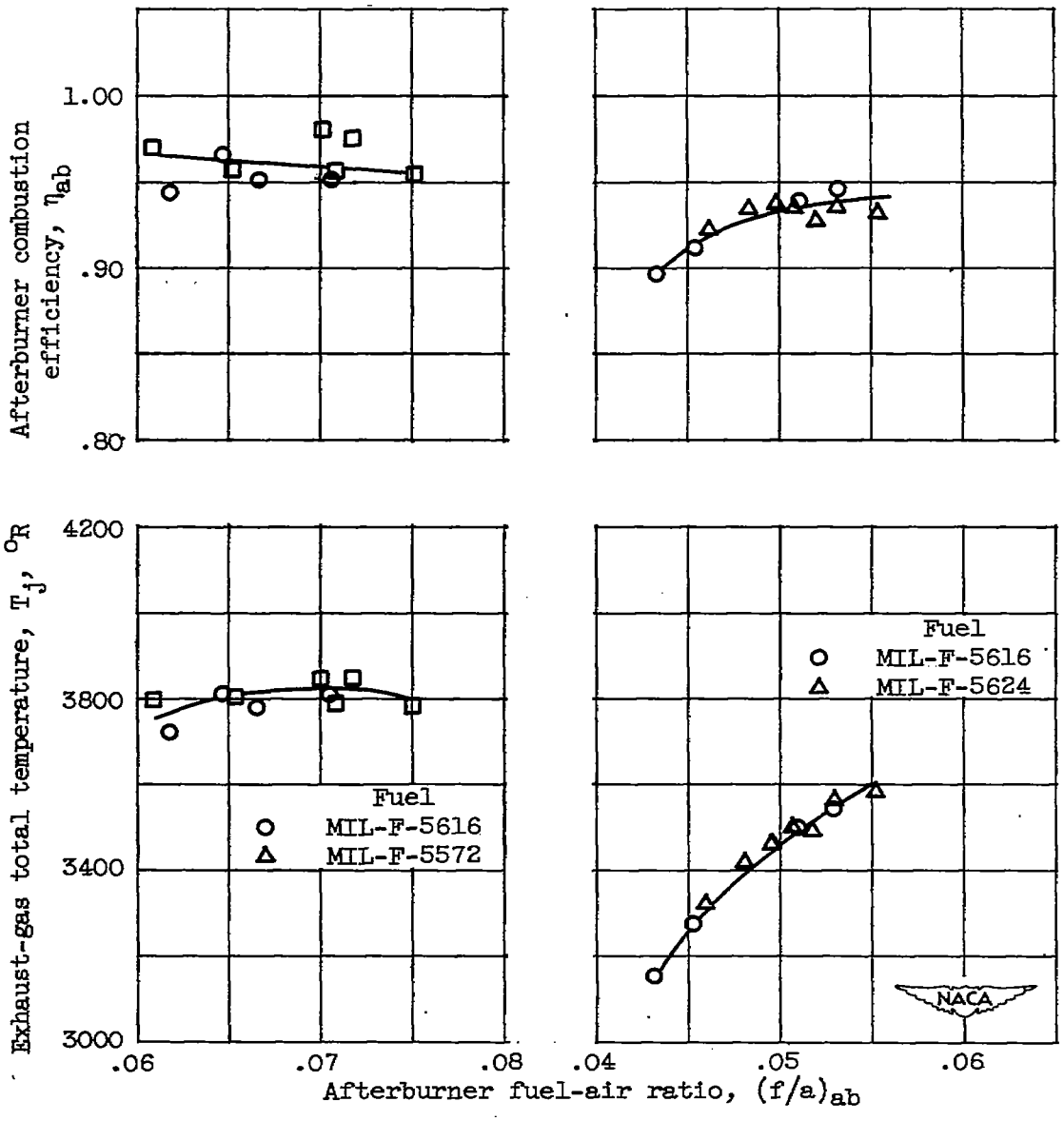

(a) Comparison of MIL-F-5616 and MIL-F-5572 fuels.

(b) Comparison of MIL-F-5616 and MIL-F-5624 fuels.

Figure 19. - Effect of fuel type on performance of two series C configurations.

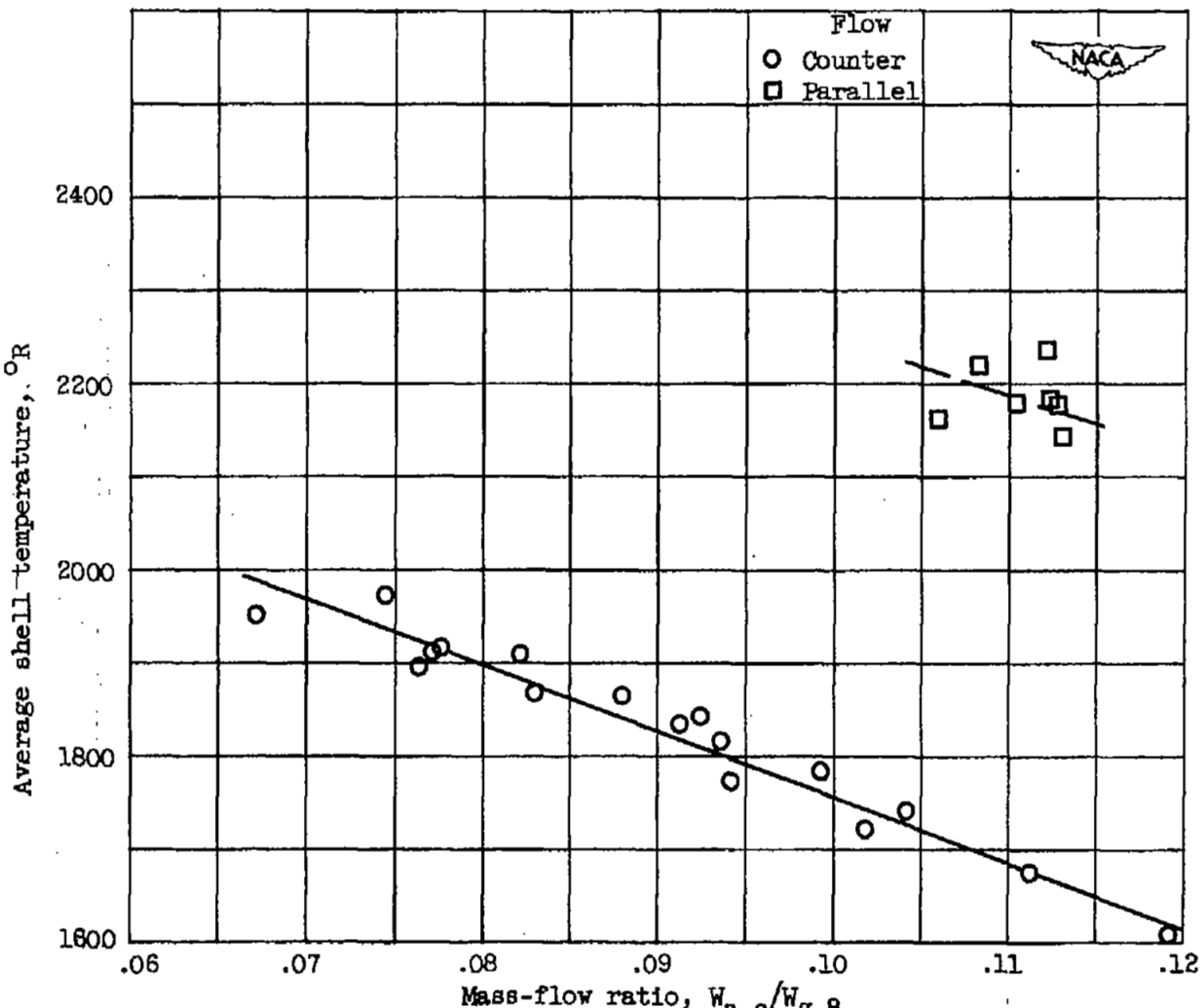

Figure 20. - Comparison of average shell temperatures obtained with counter-flow and parallel-flow cooling for mean exhaust-gas temperature of 3800° R.

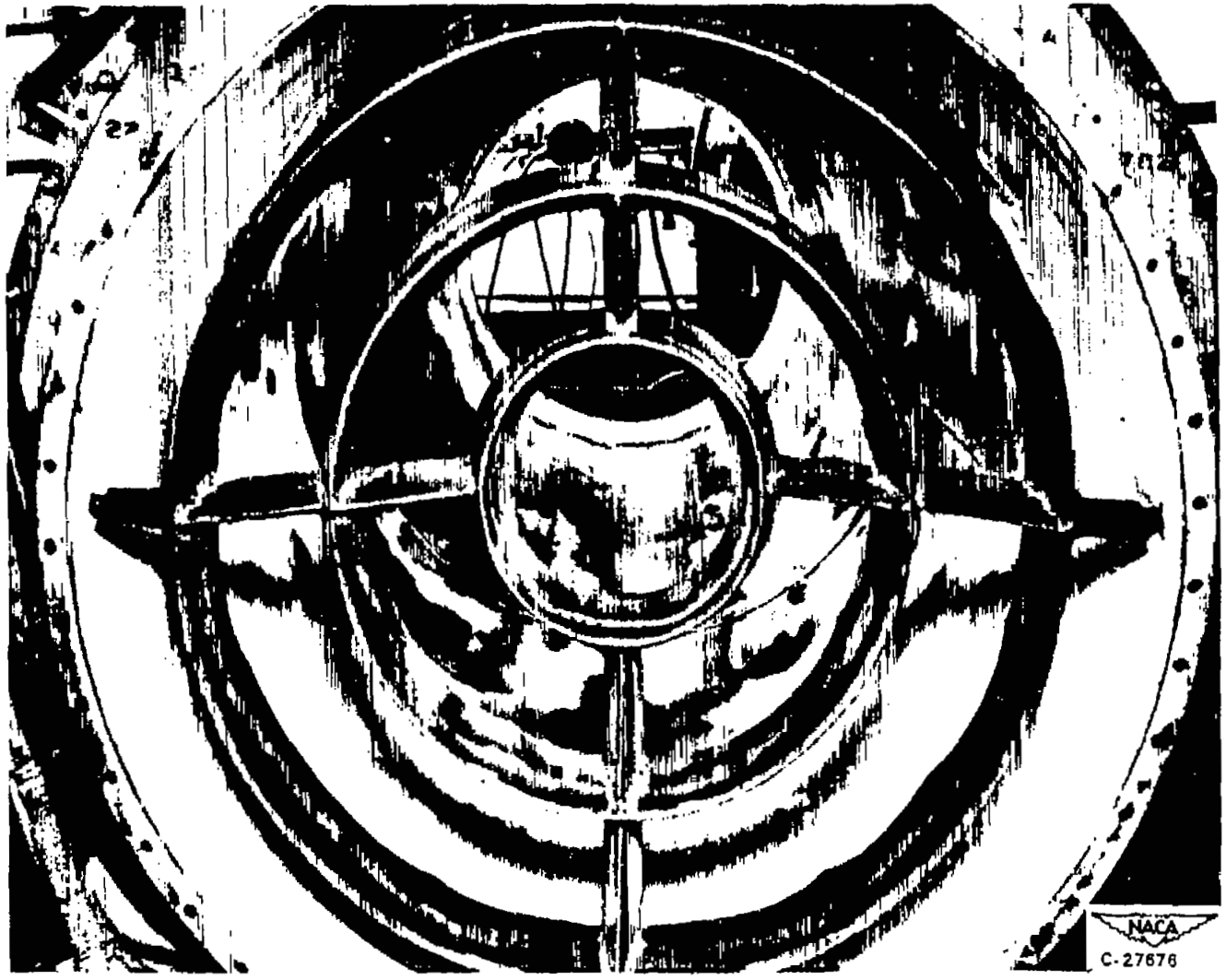

Figure 21. - Conditions of Uverite coating after 15 minutes of afterburner operation.

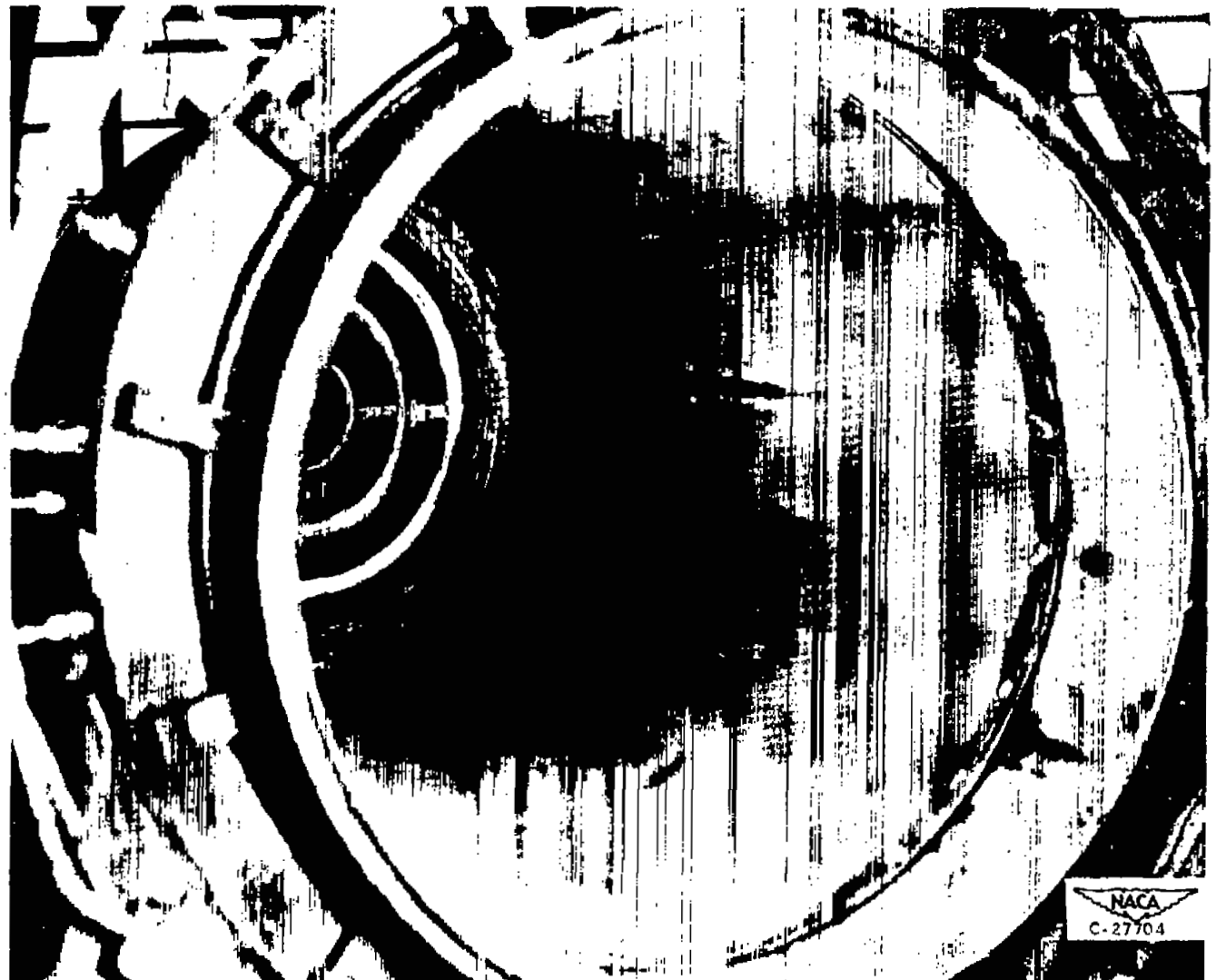

Figure 22. - Appearance of residual coating due to 4 percent ethyl silicate in the tail-pipe fuel.

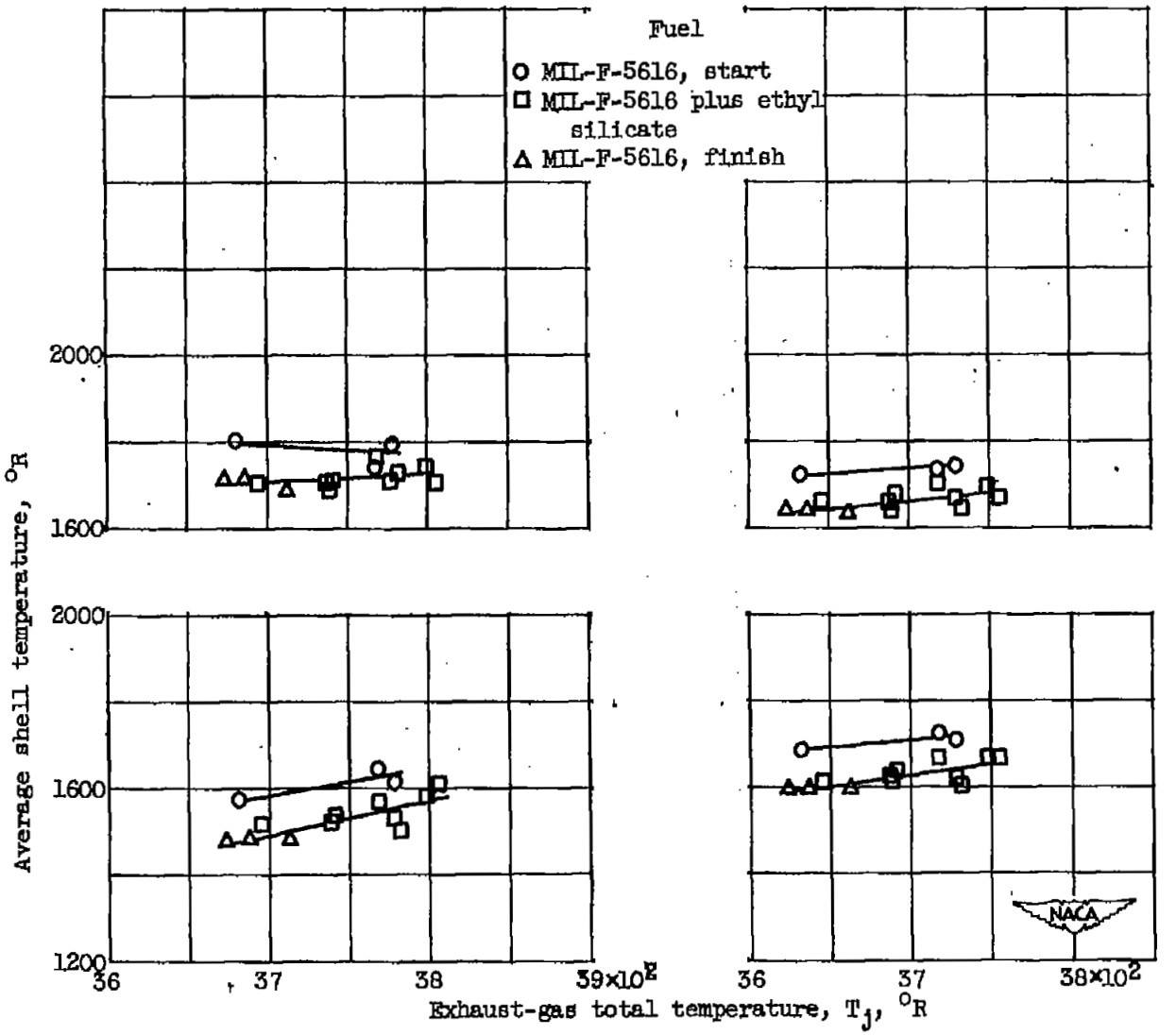

Figure 23. - Effect on shell temperatures of 4 percent ethyl silicate in fuel.

[redacted]